Università Politecnica delle Marche
Scuola di Dottorato di Ricerca in Scienze dell'Ingegneria
Curriculum in "Ingegneria biomedica, elettronica e delle telecomunicazioni"

Estrazione non invasiva del segnale elettrocardiografico fetale da registrazioni con elettrodi posti sull'addome della gestante

Non-invasive extraction of the fetal electrocardiogram from abdominal recordings by positioning electrodes on the pregnant woman's abdomen

Tesi di dottorato di
Angela Agostinelli

Tutor accademico: ***Dott.Ing. Laura Burattini***

Abstract

The heart is the first organ that develops in the fetus, particularly in the very early stages of pregnancy. Compared to the adult heart, the physiology and anatomy of the fetal heart exhibit some significant differences. These differences originate from the fact that the fetal cardiovascular circulation is different from the adult circulation. Fetal well-being evaluation may be accomplished by monitoring cardiac activity through fetal electrocardiography (fECG). Invasive fECG (acquired through scalp electrodes) is the gold standard but its invasiveness limits its clinical applicability. Instead, clinical use of non-invasive fECG (acquired through abdominal electrodes) has so far been limited by its poor signal quality. Non-invasive fECG is extracted from the abdominal recording and is corrupted by different kind of noise, among which maternal ECG is the main interference. The Segmented-Beat Modulation Method (SBMM) was recently proposed by myself as a new template-based filtering procedure able to provide a clean ECG estimation from a noisy recording by preserving physiological ECG variability of the original signal. The former feature is achieved thanks to a segmentation procedure applied to each cardiac beat in order to identify the QRS and TUP segments, followed by a modulation/demodulation process (involving stretching and compression) of the TUP segments to adaptively adjust each estimated cardiac beat to the original beat morphology and duration. SBMM was first applied to adult ECG applications, in order to demonstrate its robustness to noise, and then to fECG applications. Particularly significant are the results relative to the non-invasive applications, where SBMM provided fECG signals characterized by a signal-to-noise ratio comparable to that characterizing invasive fECG. Thus, SBMM may contribute to the spread of this noninvasive fECG technique in the clinical practice.

Fetal electrocardiography: extraction of the non-invasive fetal electrocardiogram

High-risk pregnancies are becoming more prevalent. The possible causes of complicated pregnancies can be preterm delivery, fetal oxygen deficiency, fetal growth restriction, or hypertension [1-3]. Early detection of these complications is fundamental to permit timely medical intervention, but is hindered by strong limitations of existing monitoring technology. The most common method to monitor the fetal health condition is cardiotocography (CTG), i.e. the monitoring of the fetal heart rate (HR) and its variability (HRV) in response to the utero activity [4]. Currently, in obstetrics practice, fetal HR is obtained by two different ways: non-invasively by a (Doppler) ultrasound probe on the maternal abdomen, or, more rarely, invasively by an electrode fixed on the fetal scalp [5]. The first is relatively inaccurate but is non-invasive and applicable in all stages of pregnancy [6]. The latter is more accurate but it can be applied following rupture of the membranes and sufficient dilatation, restricting its applicability at only the last phase of pregnancy [5]. Also, besides the accuracy issue, CTG has a high sensitivity but a low specificity [4]. This means that in most cases of fetal distress, CTG reveals specific patterns of HRV, but these patterns can also be revealed for healthy fetuses. Consequently, the result is a complicate diagnosis of the fetal conditions. Thus, to prevent not necessary interventions, additional information to CTG are required. Monitoring of the fetal health condition by the fetal electrocardiogram (fECG), as a supplement of CTG, provides an added value due to the more information which can be derived from fECG morphology [7]. Unfortunately, the application of fECG in obstetrical diagnostics is limited because at present fECG can only be reliably measured by an invasive scalp electrode. To overcome this limited applicability, many attempts have been made to record a non-invasive fECG by applying electrodes on the maternal abdomen, but these attempts have not yet led to approaches that permit widespread clinical application [5]. This is due to the low signal-to-noise ratio (SNR) which characterized the non-invasive recordings. From a mathematical point of view, the non-invasive recording can be considered as a summation of three components:1) fECG (or signal of interest), 2) maternal ECG (or primary

interference) and 3) noise of physiological or not physiological nature. These components have the same frequency content (about 0,5-100 Hz) and then, they result overlapped in frequency. To extract the signal of interest, such as fECG, traditional linear filtering cannot be applied because works under fixed bands. Thus, further signal processing techniques are required. Many techniques have been proposed for fECG extraction and can be summarized in linear or nonlinear decomposition techniques (among which the independent component analysis is the most commonly used), template subtraction and adaptive filtering. Thus, the aim of this thesis is to propose the extraction of fECG signal from the non-invasive recording by a new template-based technique, called Segmented-Beat Modulation Method (SBMM) [8-11]. SBMM is developed and implemented at the Department of Information Engineering of the Polytechnic University of Marche. Covered by Italian patent, now is waiting for international extension. Differently to common template-based techniques present in the literature, SBMM is able to reproduce the regular physiological ECG variability from which it is possible to derive clinically useful information. At first proposed for ECG estimation from noisy recordings, SBMM was applied to fECG estimation from the non-invasive recordings.

Chapter 1

Physiological background

In this chapter, the physiological background of fECG signal is covered. In addition, several parameters that can be derived from the fECG are discussed. Although this chapter deals about of the clinical evaluation of fECG, it does not present an overview of the state-of-the-art of signal processing techniques for extracting and analysis of the fECG. These techniques are discussed later in more detail.

1.1 Physiology of the fetal heart

Development of fetal heart

The heart is the first organ that develops in the fetus, particularly in the very early stages of pregnancy [12] (see Fig. 1.1). Already between 3th and 7th week after fertilization, a simple tube assumes the shape a four-chambered heart, as shown in Fig. 1.2. Generally, the heart begins to beat by the 3rd week of life and the blood is pumped in a separate closed circulatory system. Between 7th to 9th week, the fetus can be externally monitored by ultrasound imaging, even if the quality of these images is not excellent. In addition, the ultrasound imaging cannot measure the cardiac waveforms and beat-to-beat variability of HR. At 20th week, the fetal heart can be heard and usually is characterized by a frequency between 120-160 bpm. At 6th week of gestation, brain waves can be recorded, the skeleton is completed and most reflexes are present. However, the embryo is only 0,5 cm long. Between the 12th and 14th week of gestation, when the fetus weighs around 30 gr and is about 7 cm long, the muscles begin to develop and spontaneous movements can be observed. Only at 26th week, the fetus begins to inhale and exhale. Of course, the fetus is not breathing air and the blood oxygenation follows a separate circle. The normal gestation time is approximately 40 weeks [13]. Although the fetus is capable of living outside the womb already from 23th-24th week, this would be considered premature at

birth. Indeed, at 23th week the chance of viability outside of womb is around 15%, while it rising (around 56%) at 24th weeks and (around 79%) at 25th week.

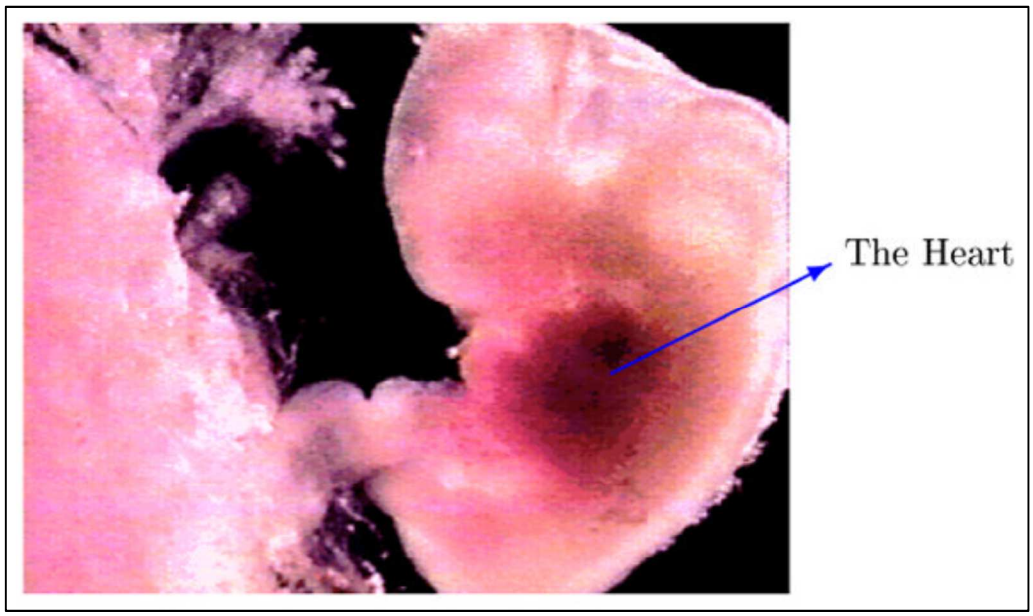

***Fig. 1.1**. The fetus and its heart in the early stages of development [14].*

Feto-maternal compartment

Fig. 1.3 show the simplified anatomy of the feto-maternal compartment. The fetus is surrounded by several different anatomical layers with different electrical conductivities [15], as reported in Table 1. The highest and lowest conductivity are found in the amniotic fluid and the vernix caseosa, respectively. Both these layers surround the fetus completely. In maternal abdomen compartments, the skin and the subcutaneous fat have a poor conductivity (about ten times smaller than the muscle tissue [15]). However, these two layers represent the interface between the electrodes and the internal tissue and have considerable influence on the recorded fECG. All of these different tissues and layers consist a so-called volume conductor, in which the fetal cardiac signals propagate up to the maternal body surface. The volume conductor is not constant. During the gestation, its electrical conductivity and its geometric shape continuously vary. Particularly, in the second half of gestation (from 20th week onward) when the amniotic fluid, the placenta and the fetus itself are all increased in volume [16]. The vernix caseosa (layer at very low conductivity) forms between 28th and 32nd week of gestation [15], and electrically shields

the fetus. However, the fECG recording on the surface of the maternal abdomen become very difficult. In normal pregnancies, the vernix caseosa slowly dissolves between 37th and 38th week of gestation [15].

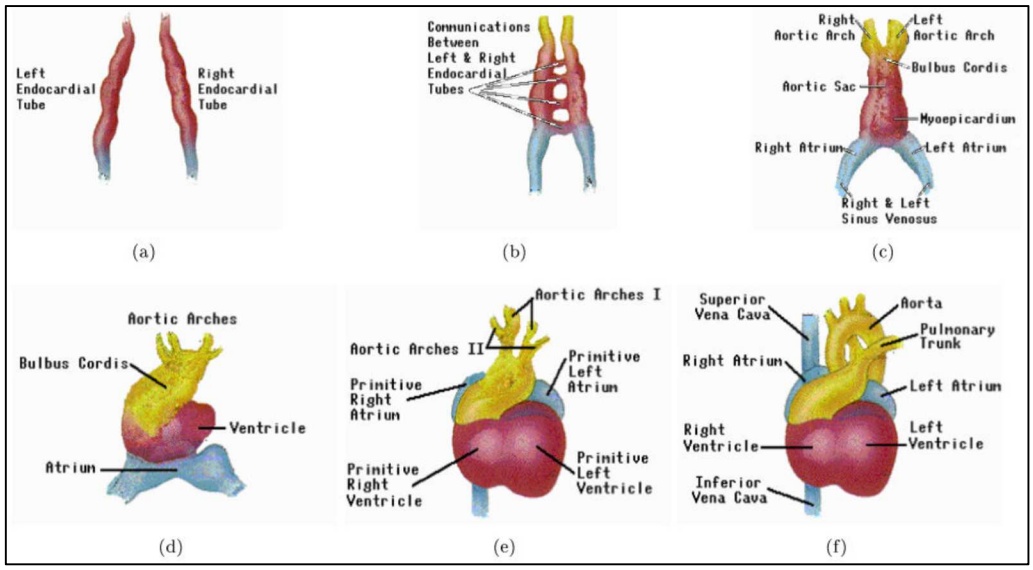

***Fig. 1.2**. Development of the fetal heart during gestation in chronological order (from a to f) [14].*

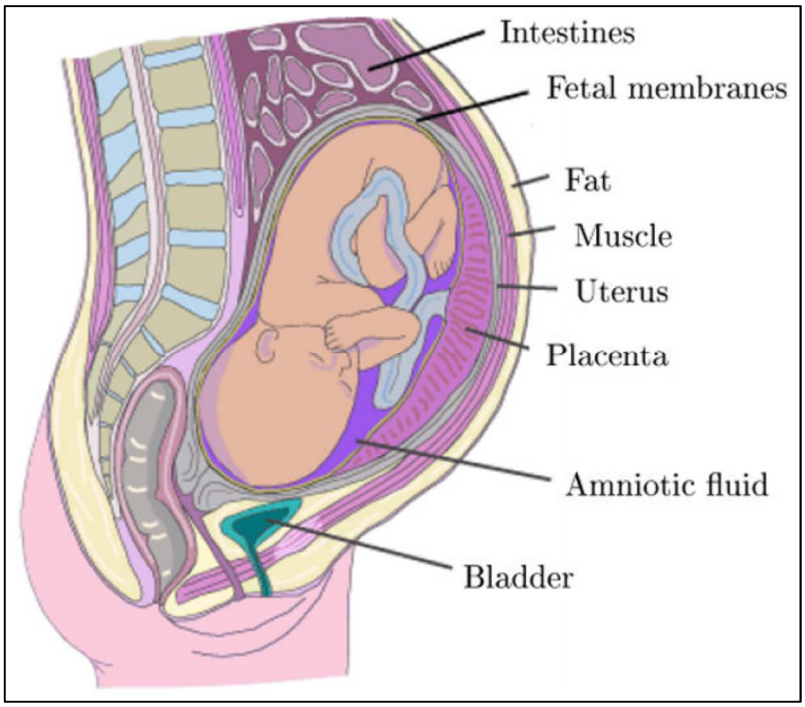

***Fig. 1.3**. The major feto-maternal compartment that influence the fetal cardiac surface potentials [14]*

Fetal presentations

During the first two trimesters of pregnancy, the fetus has not a specific presentation and moves about a lot. By the middle of the third trimester, the fetus commonly settles in a head-down position known as the vertex presentation, which is more appropriate for birth [17]. However, as shown in Fig. 1.4, the fetus may also settle in other less probable presentations. The presentation of the fetus influences the fetal cardiac signals recorded from the maternal body surface over different leads [18].

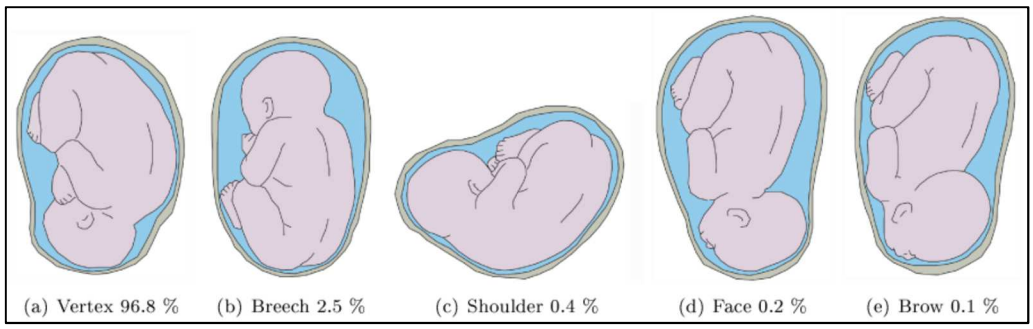

***Fig.1.4**. Different fetal presentations and the percentage of incidence at the end of gestation [14]*

Anatomy of the adult heart

The adult heart is a muscular organ that consists of two separate pumps (right and left pumps) [19]. The right pump pumps the blood through the lungs and the left pump pumps the blood through the peripheral organs. Each of these parts is composed of two chambers: an atrium (upper) and a ventricle (lower). While the atrium helps the blood to move into the ventricle, the ventricle thrusts the blood through the pulmonary or peripheral circulation. The heart has a specialized system for generating rhythmical impulses, which cause rhythmical contractions of the heart muscle, and conducting these impulses rapidly through the heart. When this system normally works, atria contract a few moments ahead of ventricles by allowing the filling of ventricles, before they thrust the blood through the lungs and peripheral circulation. The fibers of this specialized conducting system have the capability of self-excitation, a process that cause an automatic rhythmical discharge and the subsequent contraction. The fibers of the sinoatrial (SA) node exhibit this capability in largest extent and, therefore, the SA node normally controls the rate of contractions of the complete heart. Particularly, the fibers of SA node contract

and the generated impulses subsequently propagate through the heart. After the depolarization, the cell exhibits a refractory period and no excitation can occur. At the end of the refractory period, the SA node is again the first to self-excite, and for this reason, the SA node is responsible for the of contractions of the heart. The fibers of SA node trigger an action potential that propagates rapidly through both atria and from there through the His (or atrioventricular- AV) bundle into the ventricles. The His bundle is the one that mainly delays the transmission of action potentials from the atria into the ventricles, by allowing time for the atria to empty their contents into the ventricles before ventricular contraction begins. Fig. 1.5 shows an illustration of the conduction path of action potentials through the heart. The distal part of His bundle passes downward in the ventricular septum and splits into two branches (left and right bundle). Each branch spreads downward to the apex of the ventricle, by progressively splitting into smaller branches that spread around each ventricular chamber and back towards the base of the heart. In addition, each part of His bundle ends with Purkinje fibers that become continuous with the cardiac muscle fibers. These fibers have characteristics quite opposite of those of the AV node. In order to allow all ventricular muscle fibers to contract almost simultaneously, the cardiac impulse has to appear at each muscle fiber at approximately the same time. For this reason, the Purkinje fibers are relatively large fibers that transmit the action potentials at velocities about six times larger than transmission velocities in cardiac muscle fibers.

Anatomy of the fetal heart: differences with respect to the adult heart

Relative to the adult heart, the physiology and anatomy of the fetal heart exhibit some significant differences. These differences originate from the fact that the fetal cardiovascular circulation is different from the adult circulation [20-22] (see Fig. 1.6). In the adult, gas exchange (i.e. the secretion of carbon-dioxide from the blood and the input of oxygen in the blood) takes place in the lungs [19]. From the lungs, the oxygenized blood flows through the left part of the heart into the peripheral circulation. Since this peripheral circulation is larger than the pulmonary circulation, the left ventricle has to generate a substantially higher pressure than the right ventricle to ensure sufficient perfusion to the organs. Consequently, the muscular mass of the left ventricle is larger than the mass of the right ventricle. In the fetus, gas exchange takes place in the placenta [23]. As a result, the fetal blood circulation works differently from the adult. First of all, the left and right parts of the fetal heart are connected by the foramen ovale and ductus arteriosus (see Fig. 1.6). The foramen ovale is a gap in the septum that divide both sides of the heart, while the

ductus arteriosus is a switching between the pulmonary artery and the aorta. Because of these interconnections, the left and right ventricles both generate the same pressure. However, in the fetal circulation, the right ventricle is responsible for about 60% of the total cardiac output whereas the left ventricle responds for the remaining 40% [20]. As a result of this higher output, the right ventricle of the fetal heart has a muscular mass exceeding that of the left ventricle.

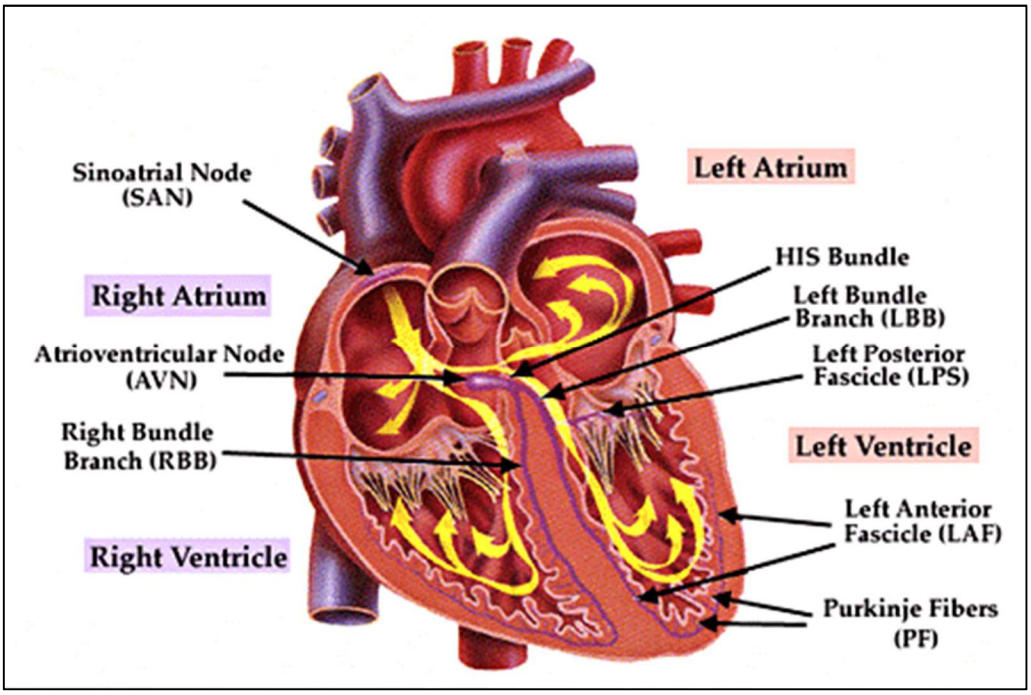

***Fig. 1.5**. Basic anatomy of the human adult heart with the main components of the action potential conduction system indicated.*

1.2 Origin of the electrocardiographic signal

Cardiac activity at cellular level

At rest, the potential of the intracellular fluid is negative with respect to the potential of the extracellular fluid [19]. This is caused by the different concentrations of Na^+, K^+, and Ca_2+ across the cell membrane. When an action potential propagates along the cell, this action potential causes an increase in the Na^+ permeability of the membrane. Consequently, a large number of Na^+ ions flows into the interior of the cell by reversing

the potential of the intracellular fluid with respect to the potential of the extracellular fluid. The cell is then depolarized. Besides the increase in Na^+ permeability, the propagation of the action potential also causes an increase in the K^+ and Ca_2^+ permeability. These permeability increases force the K^+ ions to flow from the interior of the cell to the extracellular fluid and force the Ca_2^+ ions to flow from the exterior to the intracellular fluid. However, the increase in K^+ and Ca_2^+ permeability arises more gradually than the increase in Na^+ permeability. In addition, Ca_2^+ permeability decreases earlier than K^+ permeability. Thus, the intracellular potential first rapidly increases to positive values due

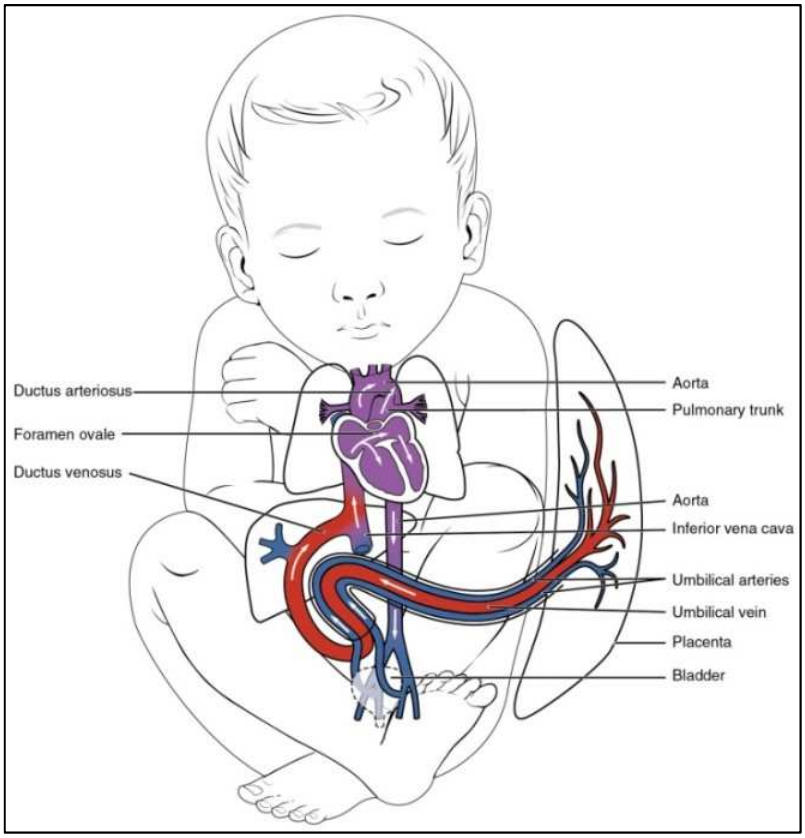

Fig. 1.6. *Basic anatomy of the human fetal heart with the main differences with respect to the adult heart.*

to the Na^+ inflow. Subsequently, the potential remains at a plateau for a short while due to the inflow of Ca_2^+ and outflow of K^+ ions. Finally, the potential returns to its rest value due to the persisting outflow of K^+ ions. Thus, the cell is repolarized. In fact, towards the end of the plateau, K^+ permeability increases to also ensure a rapid return to the rest potential. It should be noted that only cardiac cells behave as descripted above. Moreover,

also the nodal cells, which are responsible for the self-excitation of the heart behave differently [19]. Generally, propagation of the electrical impulses from cell to cell can occur in passive or active way. Passive propagation consists of the electrical conduction of impulses that are too small to cause the depolarization of the cell. In this case, the cells work as a coaxial wire that conducts the impulse but gradually reduces the impulse amplitude due to leakage currents to the cell membrane. Instead, active propagation occurs without degradation of the impulse amplitude because the depolarization of a particular cell causes an impulse in the adjacent cell that starts the depolarization of cell.

Cardiac activity at tissue level

Next to effects at the cellular level, the propagation of the action potential has also effects at the tissue level. Indeed, the contraction of the heart needs to be converted to mechanical activity. This conversion is accomplished in two steps: 1) the electrical impulse starts a chemical process that 2) in turn starts the mechanical activity [19]. The propagation of the action potential causes the release of large quantities of Ca_2^+ ions from the sarcoplasmic reticulum into the myofibrils (see Fig. 1.7). Then, the attractive forces between the actin and myosin filaments are involved by causing the scrolling of these filaments on themselves. This is the actual contraction of the muscle. Besides this mechanical effect, the propagation of the action potentials also has an electrical effect on the tissue. As mentioned before, the depolarization of a particular cell causes a potential difference compared to the adjacent cells that are not yet depolarized. Consequently, the border between a depolarized cell and a cell at rest acts as a dipole. Moreover, as the action potentials rather uniformly propagate through the cardiac tissue, adjacent fibers virtually simultaneously depolarize; and thus, the depolarization wave travels through the heart.

Cardiac activity at cutaneous level

In general, the tissues surrounding the traveling dipole are conductive, and the depolarization wave acts as a source of circular current. These currents spread in all the body surface and the skin impedance causes potential differences [24]. As the depolarization wave travels through the cardiac tissues, the potential at a specific position on the skin is not constant but varies with the traveling dipole. The representation of the skin potential as a function of time is called the ECG signal and can be measured by positioning electrodes on the skin [19].

1.3 Characteristics of the electrocardiographic signal

The ECG is a representation of the skin potential as a function of time. Indeed, the use of the word "potential" is not completely correct in this context because ECG generally constitutes a representation of the potential difference between two electrodes [19]. ECG can be described by means of a few characteristic waves (P, Q, R, S, T, and eventually U), which are associated with specific physiological events; segments (PR and ST) and intervals (PR and QT) between these waves. Fig. 1.8 shows an example of a typical ECG signal. Particularly, the P-wave is associated with the depolarization of the atria [19]. When the atria are completely depolarized, the electrical field generated by the traveling dipole is zero and the ECG consequently has zero amplitude. This isoelectrical period lasts until the action potential has propagated through the AV bundle to the Purkinje fibers and,

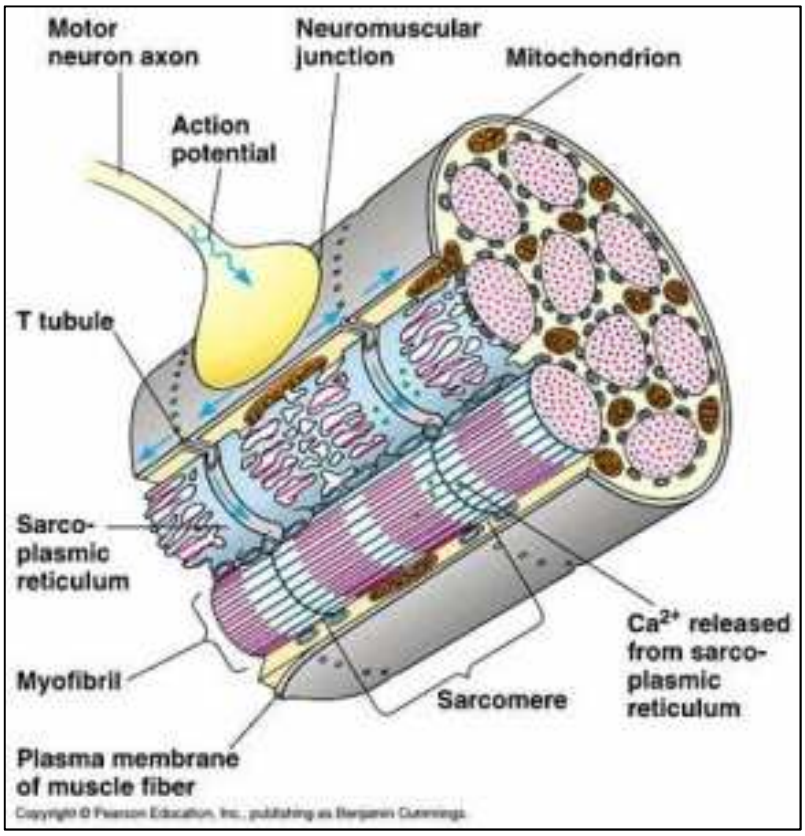

***Fig. 1.7**. Schematic view of a muscle fiber with the main components involved in the contraction.*

in the signal, is represented by PR interval. QRS complex is associated with ventricular depolarization. The amplitude of QRS complex exceeds the amplitude of P-wave drastically because the amount of muscle fibers in the ventricular walls is much larger than the amount of muscle fibers in the atrial walls. The reason for this is that the ventricles pump the blood into the peripheral circulation whereas the atria pump the blood only into the ventricles. As a result of this and because the atrial repolarization coincides with the ventricular depolarization, the repolarization of the atria cannot be distinguished in ECG. After that the ventricles are completely depolarized, the electrical field is again zero and the ECG has zero amplitude. The repolarization wave of the ventricles propagates in the opposite direction to the depolarization wave and is represented in the signal by T-wave. Because of the reversed propagation direction and the inversion of the signs in the resulting depolarization wave, T-wave has the same polarity of the QRS complex. Besides as the aforementioned potential-difference between two electrodes, ECG can also be considered as the projection of the electrical field generated by the traveling dipole in the lead vector that describes the positions of the involved electrodes with respect to one another [25]. Thus, it can be said that ECG is a one-dimensional projection of the three-dimensional electrical field generated by the traveling dipole.

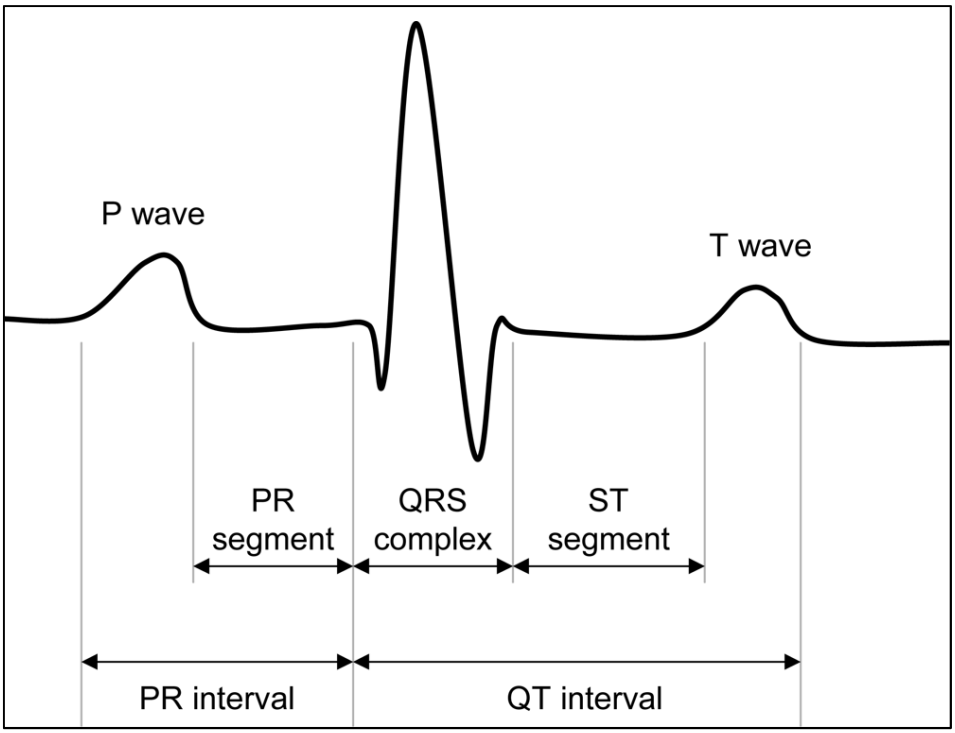

***Fig. 1.8**. Electrocardiographic (ECG) signal*

Cardiac vector

The traveling dipole produces a varying electrical field in the heart, which a first approximation can be described by a single vector: the cardiac vector [25,26]. When the orientation of the cardiac vector on the cutaneous level is perpendicular to the lead vector between two electrodes, both these electrodes measure the same electrical field amplitude and hence the bipolar ECG amplitude is zero. In other words, the projection of the cardiac vector into the lead vector determines the instantaneous ECG amplitude. This is illustrated in Fig. 1.9, in which the three vectors composing the triangle are the lead vectors and the amplitude of the ECG is determined by the amplitude of the projection of instantaneous cardiac vector into these lead vectors [27]. In addition, this relation between the electrical field, the lead vector, and the ECG amplitude implies that the varying electrical field can be used to describe the ECG at the body surface. Consequently, one of the main interests in fECG monitoring is the description of this electrical field vector over time: the fetal vectocardiogram (VCG) [28]. Generally, the fetal VCG is the three-dimensional representation of the time-path of the cardiac vector during one cardiac cycle [29]. Fig. 1.9 shows a two-dimensional illustration of the fetal VCG. In fact, this represents a simplification of the actual physiology. As the cardiac vector originates from the dipole wave, the origin of the vector travels with this wave through the heart. In the simplification used in the definition of the fetal VCG, however, the origin of the cardiac vector remains stationary [30]. In general, the fetal VCG consists of three closed loops associated with atrial depolarization, ventricular depolarization, and ventricular repolarization [28]. The ventricular depolarization loop (the largest of these loops) exhibits one particular direction for which the cardiac vector has maximum amplitude. This direction is referred to as the electrical axis of the heart or the main heart axis [19]. For adults, the main heart axis is on average tilted 57° with respect to the transverse plane, i.e. approximately corresponding to the direction from the right shoulder to the left ankle (Einthoven lead II), but deviations from -30° to 90° are considered normal [19].

1.4 Characteristics of the fetal electrocardiographic signal

The fetal heart is among the first organs that develop in the fetus and, after 7 weeks of gestation [5], is characterized by an anatomic conformation similar to that of an adult heart (four cameras, two atria and two ventricles) [14]. Consequently, from a

morphological point of view, fetuses and adults have rather similar ECG signals containing the same basic waves: P wave, associated to atrial depolarization; QRS complex, associated to ventricular depolarization; and T wave, associated to ventricular repolarization. Still, the mechanical function of the fetal heart differs from that of the adult heart because of some structural differences required by a different blood circulation in the prenatal period. After birth, the left ventricle pumps blood into the body for delivering oxygen whereas the right ventricle pumps blood into the lungs for acquiring oxygen. As above said, in the fetus the oxygen is supplied by the placenta [31] and therefore blood is not pumped into the lungs for this purpose. Both ventricles pump blood throughout the body (including the lungs). Particularly, the left ventricle supplies blood to the heart itself and to brain, whereas the right one to all the inferior parts of the body. The cardiac output

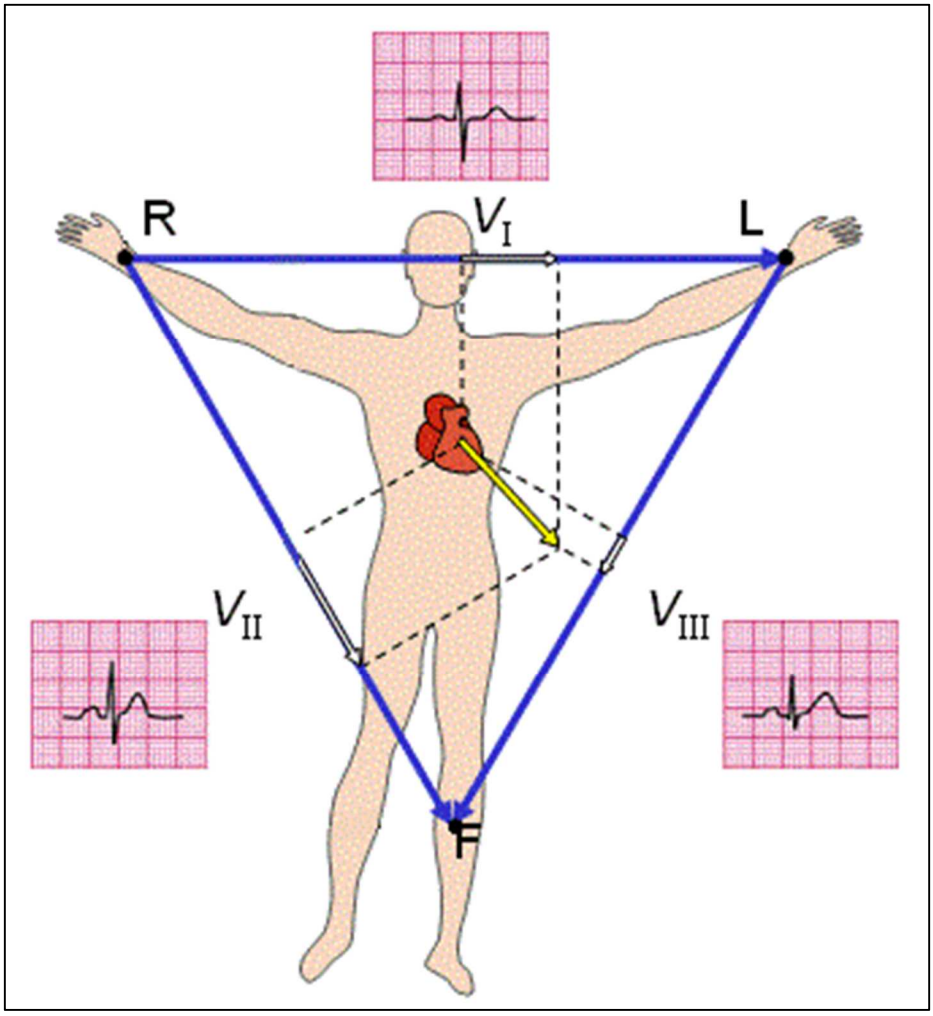

***Fig. 1.9**. Two-dimensional illustration of the vectocardiogram (VCG, in yellow) and the instantaneous projection of the cardiac vector.*

of the right ventricle is greater than that of the left ventricle and this yields an abundance of cardiac muscle in the right part of the fetal heart. Thus, in the fetus the cardiac electrical axis is direct toward the right ventricle [14], whereas in the adult it points toward the left ventricle (which is the ventricle with the largest mass [22]). Consequently, the fetal VCG, which is the vector that indicates the magnitude and direction of the electrical forces generated by the heart during one complete cycle [31]) is oriented differently from the adult VCG, and each fECG representation (which is the projection of the fetal VCG into the appropriate lead vector) differs from the corresponding adult ECG representation [31].

Clinical Information from fetal electrocardiographic signal

Several clinical evaluations, not necessarily directly related to the fetal heart, can be derived from the analysis of the fECG signal. Several parameters of the fECG complex can be associated with the fetal condition [5,31] and below the most common ones are reported. For instance, the dimensions of the fetal heart and hence the size of the fetus can be estimated from the lengths of the intervals in the ECG, while also indications for fetal oxygen deficiency can be discerned.

Fetal Growth Parameters

Intrauterine growth restriction (IUGR) refers to poor growth of a fetus in the mother's womb during pregnancy. In this pathological state, the fetus is at risk of hypoxia [1], condition which is associated with increased perinatal morbidity and mortality and consequently, the IUGR represents a major problem in the perinatal medicine. Since the fECG provides information about fetal growth rate and oxygenation [1], it can also be used for IUGR assessment. In the fECG signal, the P-wave duration and the QRS complex duration indicate the time needed for atrial and ventricular depolarization, respectively. Such intervals are determined by both the size of the cardiac muscle and the conduction speed of the action potentials. Hypothesizing the latter to be constant, each wave has a duration that depends on the dimension of the related cardiac rooms. As the heart grows proportionally to the fetus, both the P wave duration and the QRS-complex duration can be used to estimate the size of the fetal heart [5,31] and, consequently, to assess the presence of IUGR.

Supraventricular Arrhythmias

Supraventricular extrasystoles (SVES) are heartbeats that originate in the nodal cells of the ventricles rather than in the SA node [19]. In the fECG signal, the occurrence of SVES

is shown with a widened QRS complex of opposite sign, while the P-wave, representing contraction of the atria, is absent. In most cases, SVES are sporadic and innocent and hence not relevant for fetal monitoring [5,31]. However, in the cases in which SVES are due to congenital heart diseases (like the supraventricular tachycardia, bradycardia or premature atrial contractions [32,33], fECG visualization could become of vital importance. since permits timely detection of the congenital fetal heart disease and its treatment during pregnancy or immediately after birth.

ST Segment Variability

The capability of the fetal heart to distribute the blood to the body depends on the critical balance between energy production and energy consumption. Normally, the availability of oxygen exceeds its request, and the fetal heart utilizes aerobic (i.e., oxygen dependent) metabolism to generate energy. In this case, the energetic balance is positive and the fECG morphology is normal. On the contrary, if the available amount of oxygen decreases and the requested amount persists, the energy balance becomes negative and myocardial hypoxian emerges [34]. In the fECG, the effect of myocardial hypoxia is commonly reflected in a morphological change of the ST segment, which becomes elevated or depressed (the Cochrane Library provides a support to interpret fetal ST waveform [35]). The fetus responds to the negative energy balance by suddenly increasing adrenalin to start glycogenolysis, a process in which stored glucose is utilized for generating energy. Changes in the ST segment will then indirectly reflect the fetal capacity of metabolic compensation [5,31].

Fetal Movements

Maternal perception of fetal movements is the oldest and most commonly used method to assess the well-being of the fetus starting from the 20^{th} week of gestation [36]. At first, the fetal movements are weary and infrequent, but in the second half of pregnancy, they become stronger, more frequent, and increasingly linked to fetal heart-rate patterns and fetal eye movements, and identify fetal behavioral states that are indicators of maturity and integrity of the fetal nervous system [5,31]. Severe and sustained reductions of fetal movements indicate fetal distress, often preceding fetal death. Fetal movements only temporally influence the morphology of the fECG, whereas fetal distress, which associates to a sustained decrease of fetal movements, causes prolonged variations of the fECG, in particular of the ST segment. Abnormalities in the ST segment persisting for longer than

15 seconds have been associated to critical fetal states, whereas shorter episodes to the fetal movements.

All the parameters discussed above illustrate that fECG monitoring can have added value compared to the electronic fetal monitoring. Not only the fetal heart rate (HR) can be assessed more accurately and more reliably, but also the fetal growth, fetal oxygenation and fetal movement parameters provide information about fetal distress. This raises the question why fECG monitoring has not been used as a standard in clinical practice since many years. One of the answers to this question is the lack of signal acquisition and processing techniques that enable determination of the fECG with sufficient accuracy and reliability in all stages of pregnancy.

Chapter 2

Non-invasive fetal electrocardiography

In this chapter, a brief overview of the fECG monitoring (invasive and non-invasive fECG) is provided with special emphasis on clinical applicability of the non-invasive fECG and analysis problems related to this signal.

2.1 Introduction to fetal cardiac monitoring: cardiotocography and invasive fetal electrocardiography

The assessment of procedures for accurately monitoring the fetal cardiac activity has always occupied a prominent role in the biomedical research because of its importance in safeguarding the life and the health of the unborn child. Indeed, congenital fetal heart defects are among the most common birth defects and the leading cause of birth deaths [2]. Moreover, several pathologies and complications, even not directly linked to the fetus heart, such as fetal hypoxia (a deprivation of an adequate supply oxygen that, if prolonged, can lead to irreversible neurological diseases), show abnormalities in the cardiac activity as side effect [3,7]. Premature diagnosis of such cardiac defects and activity abnormalities during pregnancy may allow the treatment of the pathologies in the early stages of the fetus development and may prevent a permanent disease or, in the worst cases, a fatal outcome [3]. The idea that fetal heart rate could be used to determine fetal well-being was first proposed by Killian in the 1600's [37], but it remained unnoticed until 1818 when Mayor and Kergaradec described the method of auscultating fetal heart sounds by placing the ear next to the maternal abdomen [37]. Later, Kergaradec further suggested that fetal heart sounds could be used to determine fetal viability and life [38]. In 1833, Evory Kennedy, an English physician, published a textbook on Obstetric Auscultation, mentioning the possible correlation between fetal heart rate patterns and fetal health, and

recommended auscultation of the fetal heart rate as a tool of intrapartum monitoring [39]. Improvements of such technique lead to use an acoustic sensor, the fetal stethoscope or fetoscope, capable to capture the beating activity of the fetal heart valves opening and closing [37]. This technique remained practically unchanged until the advent of electronic fetal monitoring, that has its origin in 1906, when Cremer first attempted recording of the fECG by using silver electrodes positioned on the abdomen and vagina and connected to the galvanometric apparatus [38].

Nowadays two techniques are mostly used for fetal cardiac monitoring: the CTG and the invasive (or direct) fECG. CTG consists of simultaneous recordings performed by two separate transducers, an ultrasonic sensor, that continuously emits ultrasound and detects motion of the fetal heart by the characteristic of the reflected sound, and a pressure transducer, that provides information on the uterine contractions. Although the transducers can be either external or internal, CTG is usually performed in a noninvasive fashion, with the two sensors strapped to the mother abdominal wall. For what concerns fetal cardiac monitoring, the CTG provides information regarding the fetal heart rhythm, including baseline heart-rate and heart-rate variability, accelerations, decelerations and trends. When first introduced, this practice, which became almost universal for hospital births, was expected to reduce the incidence of fetal demise in labor and cause a reduction in cerebral palsy. Still, in recent years there has been some controversy as to the utility of the CTG in low-risk pregnancies, and the related belief that over-reliance on the test has led to increased misdiagnoses of fetal distress and hence increased (and possibly unnecessary) cesarean deliveries [4]. The 4th annual Confidential Inquiry into Stillbirths and Deaths in Infancy analyzed intrapartum deaths due to asphyxia in babies weighting more than 1500 gr (Maternal and Child Health Research Consortium Confidential Enquiry into Stillbirths and Deaths in Infancy, 4th annual report 1997 CEMACH, London). The inquiry reported that the interpretation of the CTG component of obstetric care was questionable in more than 50% of deaths. This is not entirely surprising as the clinical algorithm directing interpretation of fetal heart-rate records is largely based on empirical observations of recordings in human labor. Large intra- and inter- observed differences in CTG interpretation are well-recognized even among experts [39]. In many cases of birth asphyxia, retrospective review demonstrates the ambiguity of CTG leading to a failure to recognize fetal distress. Analysis of such cases has led several countries to recommend that all staff involved in intrapartum care should receive regular training in CTG

interpretation. Invasive fECG is the second most common technique for fetal cardiac monitoring, principally used in the USA. It consists of a recording of the electrical activity of the fetal heart through the insertion of the spiral electrode on the fetal scalp (see Fig. 2.1), and thus, its applicability is limited only to the labor, because the insertion of the electrode requires the chorioamniotic membranes to be ruptured and a sufficient dilatation of the uterine cervix. Also, the presence of monitoring instrumentation in the uterine cavity penetrating the fetal skin may cause infection and fetal injury. However, compared to the CTG, invasive fECG provides much more information on heart health state since the signal morphology reflects all the phases of the fetal cardiac cycle and not only the heart rate. Indeed, in case of labor at risk, invasive fECG can be combined with the CTG, and thus we talk about "STAN" monitor [40-44]: a monitor that analyzes ST segment of the fECG and, in combination with CTG, can

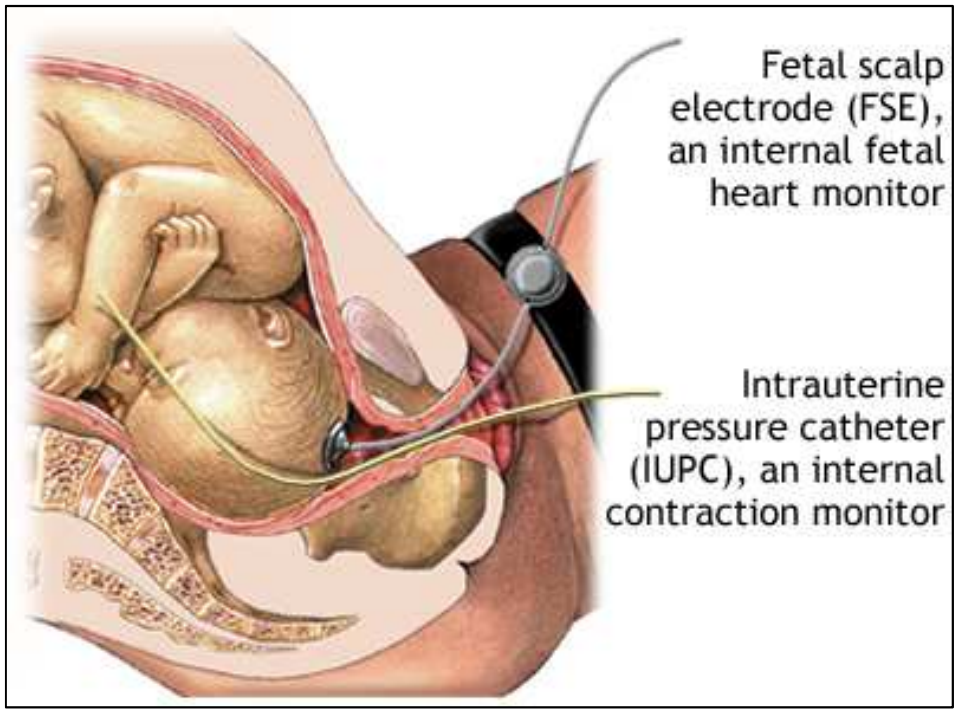

***Fig. 2.1**. Electrodes configuration for invasive fECG: insertion of the spiral electrode on the fetal scalp*

be used to assess fetal hypoxia [45]. Unfortunately, STAN can only be applied during labor since it's based on the invasively recorded fECG. Thus, in case of fetus that suffers of asphyxia before dilatation, ST analysis (evaluated by STAN) does not assess the fetal

condition correctly [40]. Generally, CTG should lead to a correct diagnosis and subsequent intervention by the physician. However, if ST analysis has already started, this potentially results in an earlier diagnosis. Then, combined with the fact that ST segment alone cannot discriminate between sustained asphyxia and normal oxygen levels [46], this address the need for a non-invasive method to record the fECG.

2.2 Non-invasive fetal electrocardiography

Non-invasive (or indirect) fECG was first attempted in 1958 by Hon [47]. It represents an alternative technique to the invasive fECG for overcoming its invasivity-related limitations. It consists of the recording of the fetal-heart electrical activity by means of electrodes positioned on the maternal abdomen [48] starting from the 37th week of gestation (see Fig. 2.2). The feature of non-invasiveness makes this kind of fECG recording a potentially promising method in the field of prenatal diagnostics. However, the abdominal measured signals include a mixture of electrophysiological signals (mostly maternal ECG but also maternal and fetal electromyograms, fetal electroencephalogram, movement artifacts) and noise. Consequently, the signal-to-noise ratio of these recordings is quite low, and detection, processing and interpretation of the non-invasive fECG are very challenging tasks. Despite has been known for over 40 years and, during these years, the several efforts to improve the signal to noise ratio of the recording [14], the non-invasive fECG technique has not yet reached reliability sufficient to be used in daily clinical practice and is still a current research topic among physicians and biomedical engineers.

Electrodes features

The non-invasive fECG signal is obtained by applying electrodes on the pregnant-woman abdomen, thus representing the interface between the woman body and the electronic measuring apparatus. Such electrodes derive the electrophysiological signal by transforming, through chemical reactions, the ionic currents (which flow in the body) in electronic currents (used by measurement electronic instruments). In order for this conversion to happen, the sensors are constituted by a metal in contact with a salt solution. The passage of electric current from the body to an electrode can be understood by considering the electrode-electrolyte interface, with the electrolyte that represents the body fluid containing ions. Then, a net current crosses the interface passing from the electrod to

the electrolyte. Electrodes can be ideally classified in perfectly polarizable or perfectly non-polarizable, depending on what happens when a current passes the electrode-electrolyte interface. When a current is applied to perfectly polarizable electrodes, no actual charge crosses the electrode–electrolyte interface. Then, the current across the interface is a displacement current, and the electrode behaves as a capacitor. Instead, when a current is applied to perfectly non-polarizable electrodes, this passes freely across

Fig. 2.2. *Electrodes configuration for the non-invasive fECG: positioning the electrodes on the maternal abdomen*

the electrode–electrolyte interface requiring no energy to make the transition. Thus, there are no overpotentials. Clearly, real electrodes can only approximate these two ideal types of electrodes [49,50]. For example, the silver/silver chloride (Ag/AgCl) electrode, widely used in electrocardiography, approaches the characteristics of a perfectly non-polarizable electrode [50] and represents a good compromise between the quality of the recorded signal and cost. Because the biopotentials are recorded from the skin surface, the sensor-skin interface has also to be taken into account. When applying an electrode on the skin, a transparent electrolyte gel containing Cl- is generally used to maintain a good contact and reduce the impact of the skin on the impedance by making its dry outer layer ion conductive [51]. Moreover, the skin area under the electrode must be slightly abraded (through the cotton imbued with abrasive paste) to remove the most superficial stratum of the skin, i.e. the stratum corneum, that is poorly conductive. Thus, the contact impedance between the sensor and the skin is minimized and the recorded signal quality is optimized.

Electrode configurations

In abdominal recordings for non-invasive fECG, the signal morphology depends not only on electrodes placement, but also on fetus position. Consequently, definition of an optimal electrodes location is not possible [49], even though some different configurations have been proposed in literature in the attempt to standardize the recording procedures (see below) [5]. Globally, electrode configurations for non-invasive fECG recordings can be grouped into two classes: pure abdominal configurations and mixed configurations (see Fig. 2.3). Differently from the former, the latter also provide pure maternal ECG tracings.

Pure abdominal electrode configurations

Configuration with four electrodes. According to this configuration proposed by Karvounis et al. [52], signals are acquired using four electrodes placed on the mother's abdomen [53-55]: the common electrode is located on the symphysis pubis while the other three are positioned in a crescent fashion around the navel (to the left, above and to the right of the navel), as to making a cross whose central point is the navel itself (Fig. 2.3 panel a).

Configuration with six electrodes. In 2012 Jezewski et al. [55] proposed to locate six electrodes: three aligned on the navel (two to the right and one to the left), one placed above the navel, a reference one on the pubic symphysis, and a common mode reference one, with activeground signal, on the left thigh (Fig. 2.3 panel b). This configuration represents a variation to the original configuration proposed in 1981 by Bergveld and Meijer [56,57], in which one electrode is positioned on the back instead that on the thigh.

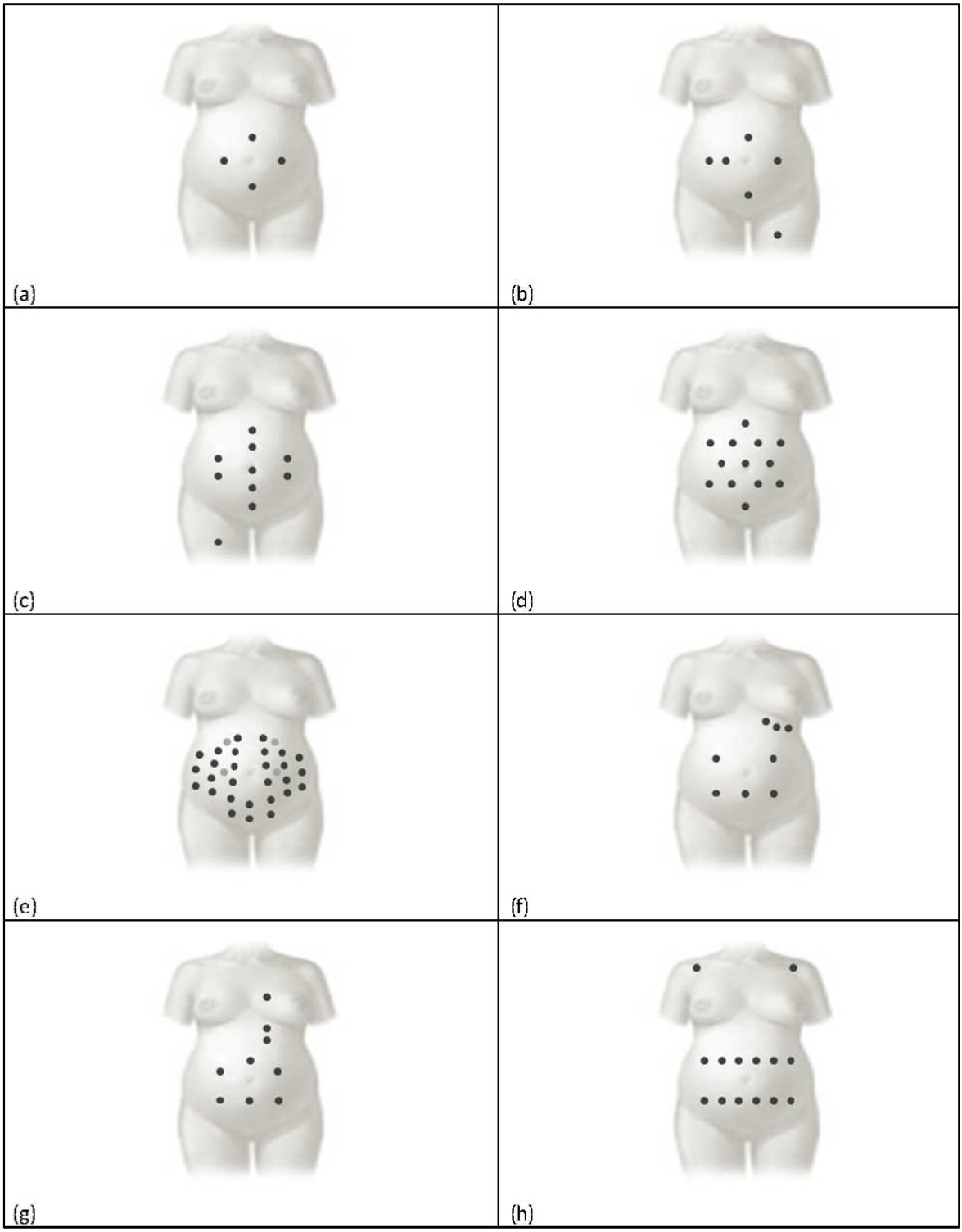

Fig. 2.3. *Electrode configurations for abdominal recordings. Pure abdominal configurations consider four (panel a), six, (panel b), ten (panel c), thirteen (panel d) and thirty-two (panel e) electrodes, respectively. Instead mixed configurations consider eight (panel f), nine (panel g) and fourteen (panel f) electrodes [5].*

Configuration with ten electrodes. This configuration, proposed by Marossero et al. [58], considers ten electrodes displaced as follows: four electrodes are vertically aligned at the center of the maternal abdomen (two above and two under the navel), two couples of electrodes are applied on the right and on the left of the line identified by the previous four, the reference electrode is placed at the abdomen center near the navel, and the ground electrode is located on the right thigh (Fig. 2.3 panel c).

Configuration with thirteen electrodes. Martens et al. [59] proposed an electrode 6-pointed star configuration characterized by the placement of 13 abdominal unipolar electrodes (Fig. 2.3 panel d). The average of all potential recorded by each electrode is considered as the common reference.

Configuration with thirty-two electrodes. This configuration, proposed by G. Clifford et al. [60], consists of a set of 32 abdominal electrodes placed on basis of anatomic landmarks (the navel, xiphoid process, pubic symphysis, axilla, and spine) to allow for an excellent coverage of the maternal abdomen, sides, and back (Fig. 2.3 panel e).

Mixed electrode configurations

Mixed configuration with eight electrodes. This configuration, presented by A. Mahmoud et al. [61], considers eight electrodes, of which five are abdominal (three around the navel and two in line with it), and three thoracic (on the left side, under the udder; Fig. 2.3 panel f) [62]. Abdominal electrode records a noisy mixture of maternal and fECG signals, while the thoracic ones detect the pure maternal ECG.

Mixed configuration with nine electrodes. Sameni et al. [63] proposed a configuration which includes nine electrodes, six abdominal ones located around the navel, and three thoracic ones vertically aligned in correspondence to the maternal heart (one above and two under the heart; Fig. 2.3 panel g).

Mixed configuration with fourteen electrodes. This 14-electrode configuration proposed by Vullings et al. [64] considers positioning 12 electrodes in two horizontal lines on the maternal abdomen, respectively under and above the navel, and one electrode on each maternal shoulder (Fig. 2.3 panel h).

Abdominal signals recorded on the maternal abdomen

From a mathematical point of view, each lead of the recording (aLead) obtained placing the electrodes on the abdomen of a pregnant woman after the 37th week of gestation can be seen as a summation of three signal components: fECG (fECG), abdominal maternal ECG (amECG), and noise (aNoise) [5]:

$$aLead = fECG + amECG + aNoise. \quad (2.1)$$

The fECG represents the signal of interest. Theoretically it is characterized by a frequency band between 0.5 Hz and 100 Hz (as shown in Fig. 2.4 [31]), even though a bandwidth of 0.5-45 Hz results usually enough for most practical applications [65-67]. Fetal QRS-complex amplitude is strongly dependent on analyzed lead, gestational age and fetus position. Typically, it does not overcome 60 μV. The amECG is the most predominant interference in the aLead. It is characterized by a frequency bandwidth similar to the one characterizing the fECG, but its amplitude can be up to 10 times higher (as shown in Fig. 2.5 [31]). Typically, maternal QRS complexes reach 100-150 μV of amplitude. Eventually, aNoise is a mixture of interferences that can or cannot have a physiological origin. It can be further decomposed in low-frequency noise (lfNoise), inband noise (ibNoise), and high-frequency noise (hfNoise): the lfNoise, characterized by a frequency band between 0 and 0.5 Hz, typically includes baseline drifts and wandering due to respiration; instead the hfNoise includes interferences that are characterized by frequency components wide above 40 Hz (till few hundreds of Hz) such as the powerline grid (50 Hz or 60 Hz), activity from the uterus and abdominal muscle activity (up to 200 Hz), and others. Eventually, ibNoise is characterized by all those noise frequency components that fall into the fECG bandwidth, and thus are the most difficult to be eliminated.

Physiological interferences

As the maternal body acts as a conductor, several other electrophysiological signals that do not originate from the fetus are recorded by electrodes [28]. Besides the amECG, these interferences include the electrohysterogram (EHG, i.e. activity from the uterus) [68,69], and electromyogram (EMG, i.e. abdominal muscle activity), as shown in Fig. 2.5. The EHG has a frequency content ranging from 0 Hz to approximately 3 Hz [70], whereas the EMG exhibits frequencies ranging from 0 Hz to 200 Hz [71]. These interferences (also with the amECG) already show the difficulty of fECG extraction and hence explain the wide range of techniques proposed to achieve this extraction.

Non-physiological interferences

Although many non-physiological interferences exist, such as imperfections in the analog-digital converter of the recording equipment, the non-physiological interferences are dominated by the powerline [72]. The interference from the powerline is centered around

50 Hz (in Italy) with harmonics at multiples of 50 Hz and can be suppressed from the composite signal by a combination of notch filters with fixed cutoff frequencies [72].

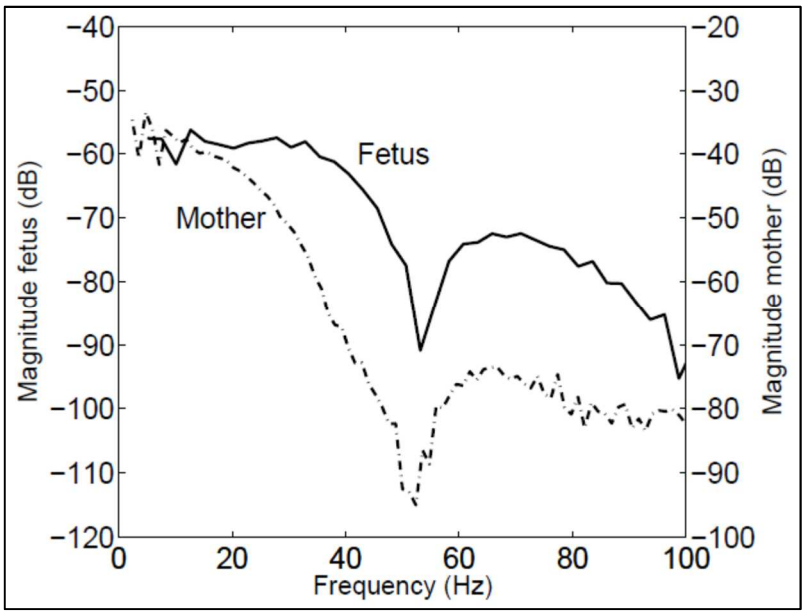

Fig. 2.4 *Frequency content of both fECG and amECG (the dip around 50 Hz is due to a notch filter to suppress the powerline interference) [31].*

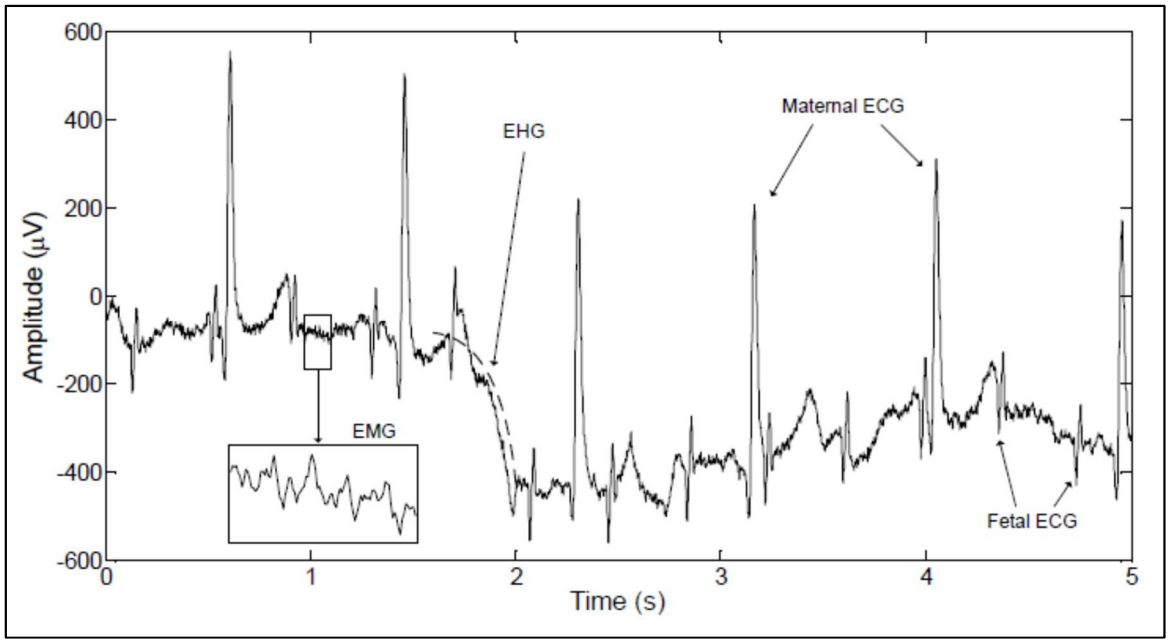

Fig. 2.5 *Segment of composite abdominal fECG recording. The contribution of the EHG is reflected by wandering of the baseline. This baseline wander is emphasized by the additionally drawn dashed arc [31].*

Volume conductor interference

In addition to the signals that corrupt the fECG in aLead, fECG analysis is complicated for another reason as well. Changes in the volume conductor between the fetal heart (on the one hand) and the abdominal electrodes (on the other hand) can distort or attenuate/amplify the fECG [73-76]. In general, these changes originate from movement of the fetus, development of the vernix caseosa [74,77], and the movement of the mother. As previously says, fetal movement is reflected in fECG as spatially correlated changes in the morphology of fECG waveform. In terms of the fetal VCG, movement of the fetus is reflected as a rotation of the VCG. However, fetal movement not only causes the fetal VCG rotation with respect to the electrode configuration on the maternal abdomen, but it also causes changes in the distance between the fetal heart and electrodes [78]. In case of electrophysiological-signals conduction (from the fetal heart to the maternal abdominal surface) not uniform, changes in distance cause both distortion and attenuation/amplification of fECG [74,76]. In case of uniform conduction, only attenuation or amplification of fECG signal is expected. Particularly, in case the fetal movement causes the decrease of distance between the heart and a particular electrode, amplification of the corresponding fECG is expected. Conversely, attenuation of fECG is caused by an increase in the heart-electrode distance. From about 28th week of gestation, the fetus develops a protective layer called the vernix caseosa [74,77,79,80]. The vernix caseosa isolates the fetus electrically from its surroundings, making virtually impossible to record a fECG on the maternal abdomen. However, from about 32th week of gestation this protective layer starts to break down, partly canceling the isolated environment and thus restoring the possibility to record fECG signal. As a consequence of this collapse of vernix caseosa, new conduction paths for the electrical signals arise [77]. These conduction paths represent a transition from uniform conduction before 28 weeks of gestation to non-uniform conduction after 32 weeks of gestation, significantly affecting non-invasive fECG recording [28]. After about 37th week of gestation, the vernix caseosa dissolves in the amniotic fluid restoring the uniform conduction characteristics of the volume conductor [74]. Thus, we can say that the limitations in fECG analysis due to fetal movement and non-uniformity of the volume conductor are mainly expected between 28th and 37th week of gestation. Another change in the volume conductor that causes fECG-signal distortions recorded on maternal abdomen is caused by fetal breathing. By filling its lungs with amniotic fluid [81], the fetus changes the impedance of conduction path from its heart to

the abdominal electrodes, affecting the recorded fECG signal. A last cause of changes in the volume conductor is the movement of the electrodes, resulting from movement of the mother. Movement of the electrodes causes the conductive layer between the skin and the electrodes to change and hence causes a change in the properties of the volume conductor. This conductive layer is generated by the thermal excitation of metallic ions in the electrode. These ions spread through the electrolyte, forming a layer balancing the electrode charge. Although the ions can move freely through the electrolyte, the speed of movement is limited and hence electrode movement is likely to disturb the electrode-skin bias [82], resulting in artifacts in the recorded fECG.

Automatic extraction of fetal electrocardiographic signal

Automatic extraction of fECG from aLead usually includes three main steps [5]: aLead prefiltration and amECG cancellation [82] (Fig. 2.6), as described below. Prefiltration of the aLead signal is usually performed in a linear fashion by application of a bandpass (0.5-45 Hz) filter. Such filter, indeed, can be seen as a cascade of a high-pass filter (cutoff: 0.5Hz) and a low-pass filter (cutoff: 45 Hz) which are finalized at attenuating lfNoise and hfNoise, respectively. The resulting filtered signal (faLead; Fig. 2.6) [5] is then composed by fECG, amECG, and ibNoise:

$$faLead = fECG + amECG + ibNoise$$

(2.2)

Usually ibNoise cannot be neglected. Typically, at most one or very few leads of a multilead recording show a signal-to-noise ratio sufficiently good (i.e., an ibNoise level sufficiently low) for a successful fECG extraction.

Several automatic procedures for fECG extraction from faLead involve amECG cancellation (see Fig. 2.6) [5]. Since the frequency bands of fECG and amECG are strongly overlapped so that linear filtering cannot be applied for their separation, but further processing techniques are required. Thus, fECG is mathematically represented by a subtraction between faLead and amECG, and the process may or may not involve amECG estimation:

$$fECG = faLead - amECG \qquad (2.3).$$

Overview on fECG extraction procedures

Many techniques have been proposed for the extraction of fECG. If pure abdominal electrode configurations are used, the extraction of fECG can occur directly from faLead by means of linear [62,83-87] or nonlinear [88-90] decomposition techniques, among which the independent component analysis (ICA) [62] is the most commonly used, or by template subtraction [57,91]. Instead, if mixed electrode configuration are used, fECG can be extracted using adaptive filtering that, in addition to faLead, also uses the mECG recorded by the electrodes located in the woman thorax or shoulder [92,93]. A detailed description of each single technique reported in literature is very hard to report here. Consequently, only technical hints of the most commonly used technique will be provided.

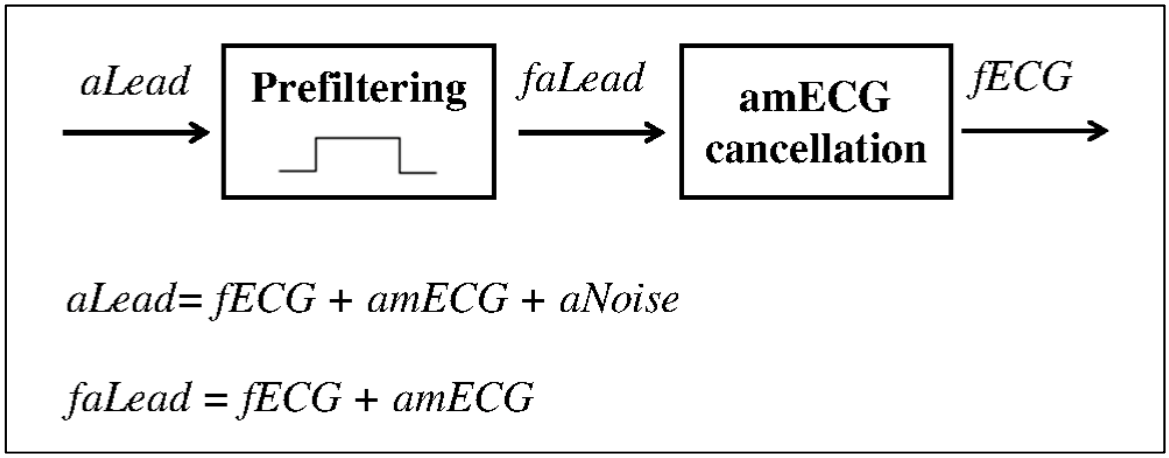

Fig. 2.6 *Automatic fECG extraction from an abdominal recording (aLead) consisting in an initial prefiltration and subsequent maternal ECG (amECG) cancellation [5].*

Independent component analysis

ICA [5] is a blind source separation technique that can be used for fECG extraction under the hypothesis of statistical independence of fECG and amECG. The ICA can be applied in case of multi-lead abdominal recording, and works under the assumption that the signals from different leads are linear combinations of the independent source signals generated by the maternal heart and fetal heart [62]. To separate the various source signals, the so called separating matrix S is used:

$$\overline{fECG} = S \; x \; \overline{faLead} \qquad (2.4)$$

where fECG and faLead are matrices containing fECG signals and faLead signals of all available leads. ICA finds the independent components by maximizing the statistical independence of the estimated components. The higher the number of available abdominal recordings, the better fECG extraction is. However, recording a large number of channels makes the procedure difficult to apply and not comfortable to the pregnant woman. Consequently, the clinical use of such approach is limited.

Template subtraction

The suppression of amECG by template subtraction [5], which can be applied to a single-lead abdominal recording, uses the repeatability of maternal ECG beats to obtain fECG [56]. The maternal beat is assumed to be an amplitude-scaled version of a common ECG beat waveform, and is called template. Maternal heart rate is hypothesized constant during the registration, so that all beats are characterized by the same length (which matches the length of the template). The calculation of the template is directly possible from the faLead, and involves various signal processing steps [91]. First, the maternal R peaks are identified using, for example, the Pan-Tompkins' procedure [94] combined with a threshold criteria finalized to distinguish maternal R peaks from fetal R peaks. Then, the segmentation of each maternal beat is accomplished in order to have the corresponding PQRST complexes which are, in the most classic approaches, averaged to get the template [56]. More rarely, the template is computed from all segmented beats using particular adaptive filters [95]. After calculation of the template, each maternal ECG beat is estimated by synchronizing and amplitude-scaling the template to the maternal beat identified in the faLead. This process can include a cross-correlation optimization. After estimation of all maternal beats, they can be concatenated to provide and estimation of amECG signal [56].

Adaptive Filtering

The extended Kalman filter [92], an extension of standard Kalman filter [96] to nonlinear systems, is usually used to perform an adaptive filtering for fECG extraction [5]. Then, the extraction of fECG from faLead with adaptive filtering needs two measurements: a primary input, represented by faLead, which contains the signal of interest and the disturbing interference (amECG), and a secondary input, represented by mECG, highly correlated with amECG. The transformation of mECG into amECG can be determined minimizing the mean square error between the primary input faLead and mECG [92]. Using neural network is another technique for adaptively extracting fECG from faLead

[93]. The input signal is considered as mECG and the target signal is faLead. The suppression of amECG from faLead occurs by correlative detraction so that the output can be considered as only fECG [95].

Clinical applications of fECG extraction procedure

Most of the studies on fECG extraction were performed by using very few recordings (few units) and were finalized to propose and validate a new algorithm. Thus, they represent methodological rather than clinical studies and significant statistics on their performances on large (of at least few tens of units) dataset of clinical data are not available. The only exception to this observation is a study that used ICA technique in 20 pregnant women [62] at 38 weeks of gestational ages to labor finalized to fetal heart rate from the fECG. The found rate of success was 85%.

Automatic processing of fetal electrocardiographic signal: features extraction

Once fECG signal has been extracted from aLead, it can be processed by applying signal processing techniques for extraction of significant feature. The fetal HR, and in particular the fetal HRV, is characterized by a specific clinical significance. Indeed, it's widely used for calculating the fetal-health parameters currently used in clinical practice. Moreover, if you use Doppler ultrasound to determine a non-invasive measure of the fetal HR, the fetal HRV is basically the only source of information available for evaluating the fetal well-being. Since HRV is controlled by the autonomous nervous system, HRV analysis can provide information on the functioning and development stage of such system. Particularly, since the sympathetic and parasympathetic parts of the nervous system operate in different bandwidths of HRV spectrum, HRV spectral analysis can provide information on both parts of the nervous system. In turn, this can provide information to assess fetal distress. To ensure accurate and reliable spectral analysis, HRV should be calculated beat-to-beat and should essentially be free from artifacts [97,98]. Generally, Doppler ultrasound devices provide an average measure (over several beats) of HR by obscuring HRV [95]. In addition, HRV calculated by Doppler ultrasound is also corrupted by noise. Usually, fetal movements lead to repositioning of ultrasound probe, and thus, in the time that passes during the repositioning, no HR data can be recorded. It causes inaccurate and unreliable spectral analysis results. Both the aforementioned problems (no beat-to-beat calculation of HRV and presence of artifacts in the data) can be solved by using fECG and thus, HRV is calculated from R peak detection. Usually, an opportunely modified version of the Pan-Tompkins' algorithm [94] is applied to identify the fetal R

peaks. A beat segmentation can also be performed either in each single fetal beat or in the fetal template constructed following a procedure analogous to the one previously described for maternal template construction. Beat segmentation allows the extraction of the features (such as P-wave duration, ST-segment elevation and QT-interval length) which provide important insights on the fetus health state.

Chapter 3

The "Segmented-Beat Modulation Method"

In this chapter, a new template-based filtering procedure for fECG extraction that is called "Segmented-Beat Modulation Method (SBMM)" is proposed. Differently from another common template-based technique present in the literature, SBMM is able to reproduce the physiological ECG variability, which provides clinically useful information on the patient's health. In addition, it has been demonstrated that SBMM is more robust to noise. At first, SBMM was proposed for ECG estimation from noisy recordings, and then it has been applied to fECG estimation from the abdominal recording, as reported in the following chapter.

3.1 Template-subtraction techniques

As previously stated, the fECG extraction involves two steps: the first step generally consists of preprocessing of the raw signal recorded on the maternal abdomen [100]. In this stage noise, artifacts, baseline wandering (i.e. trends), and power-line interference are attenuated through the use of traditional filtering. Instead, the second stage consists of the maternal ECG cancellation and then, an estimate of the maternal signal is obtained by using a form of decomposition (i.e. ICA), adaptive filtering, template generation or a combination of these three. Particularly, for approaches that use the maternal template, the template is usually obtained by averaging the maternal cardiac cycles (CC). To detect R-peak positions, automatic algorithms (such as Pan-Tompkins' procedure [94]) are generally applied. In general, under the hypothesis of knowing the R-peak positions and considering ECG as constituted by the repetition of nCC (which may differ in terms of amplitude and duration) [8], CC are obtained by considering a time window after and before R peak. If the heartbeat is known to begin with P wave, CC is more general and

may begin anywhere within ECG. Thus, the heartbeat is a specific case of CC and you consider that CC begins in PQ segment between the P-wave offset end and Q-wave onset (see Fig. 3.1), by considering Δt ms (for example, Δt=40 ms) before R peak. R-peak sequence, which contains the location of R peaks of the noisy ECG, is used to identify all CC and to compute the template as median of RR intervals. Each CC is modulated to force its duration to be exactly equal to the template. The modulated CCs are then used to compute the median CC that provides a clean template of all noisy CCs. At this point, the clean ECG is obtained by N-fold repetition of the template, after having demodulated it (by an opposite operation compared to the previous modulation procedure) in order to have its duration that matches to the duration of the corresponding noisy CCs.

3.2 The "Segmented-Beat Modulation Method"

SBMM is a denoising procedure for ECG signal which can be applied when the positions of the R peaks are known [9-11]. In first approximation, SBMM is based on the empirical observation that the duration of QRS complex depends on the duration of previous RR (i.e. on instantaneous hear-rate) and the duration of the other ECG waves proportionally vary with it [101]. Consequently, each CC can be segmented into two segments: QRS and TUP segments, as shown in Fig. 3.1.

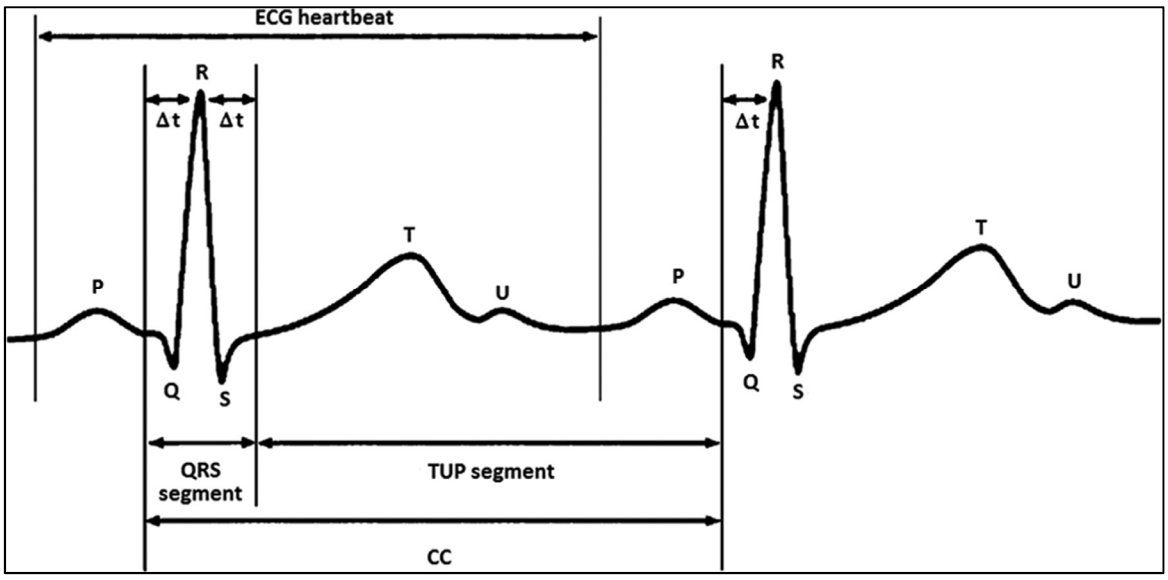

Fig. 3.1. Typical ECG waveforms and a specific CC segmented in QRS and TUP segments [8].

QRS segment (of fixed length) is identified by ΔT ms before and after the R peak, while TUP segment (of variable length) is identified within of ΔT ms after the R peak and ΔT ms before of the subsequent R peak. Thus, while QRS segment is two-times ΔT ms long (in all beats), TUP segment duration is beat dependent and equal to the difference between CC duration and QRS duration. SBMM procedure consists of two consecutive steps: 1) template computation, and 2) ECG estimation, as shown in Fig.3.2, panel a.

1. Template computation

A simplified version [8] (the detailed original in [9-11]) of the template-computation step is depicted in the upper part of Fig. 3.2 panel (b). The R-peak positions (R-peak sequence) are used to identify all CCs and to compute the median RR interval (MRR). At first, all CCs are segmented and all TUP segments are modulated by stretching or compressing, in order to have the length of CC equal to MRR. At this point, a template beat (MCC) is obtained as the median of all modulated CCs. Modulated CCs are reconstructed by using the original QRS and all modulated TUP segments.

2. ECG estimation

A simplified version [8] (original detailed in [9-11]) of block diagram of ECG-estimation step is depicted in the lower part of Fig. 3.2, panel b. To reconstruct the clean ECG tracing, the template beat is N times concatenated after demodulation (compression or stretching) of TUP segments. Number N represents the number of beats that are contained in the original noisy ECG recording. Particularly, demodulation process is performed to have the length of the estimated CC equal to the corresponding CC in the original noisy recording. Small inter-beat, nonlinear heart-rate variations of CC waveforms are compensated by using optimization processes that include cross-correlation, maximization and distance minimization between the reconstructed and the original CCs.

SBMM procedure is covered by an Italian patent, and now is waiting for the international extension.

3.3 "Segmented-Beat Modulation Method" for electrocardiogram estimation from noisy recordings

As previously stated, at first, SBMM was proposed for estimation of a clean ECG from a noisy recording [8]. In real conditions, ECG is a pseudo-periodic signal. Indeed, no ECG beat is perfectly identical to another, and it may vary in terms of morphology and duration.

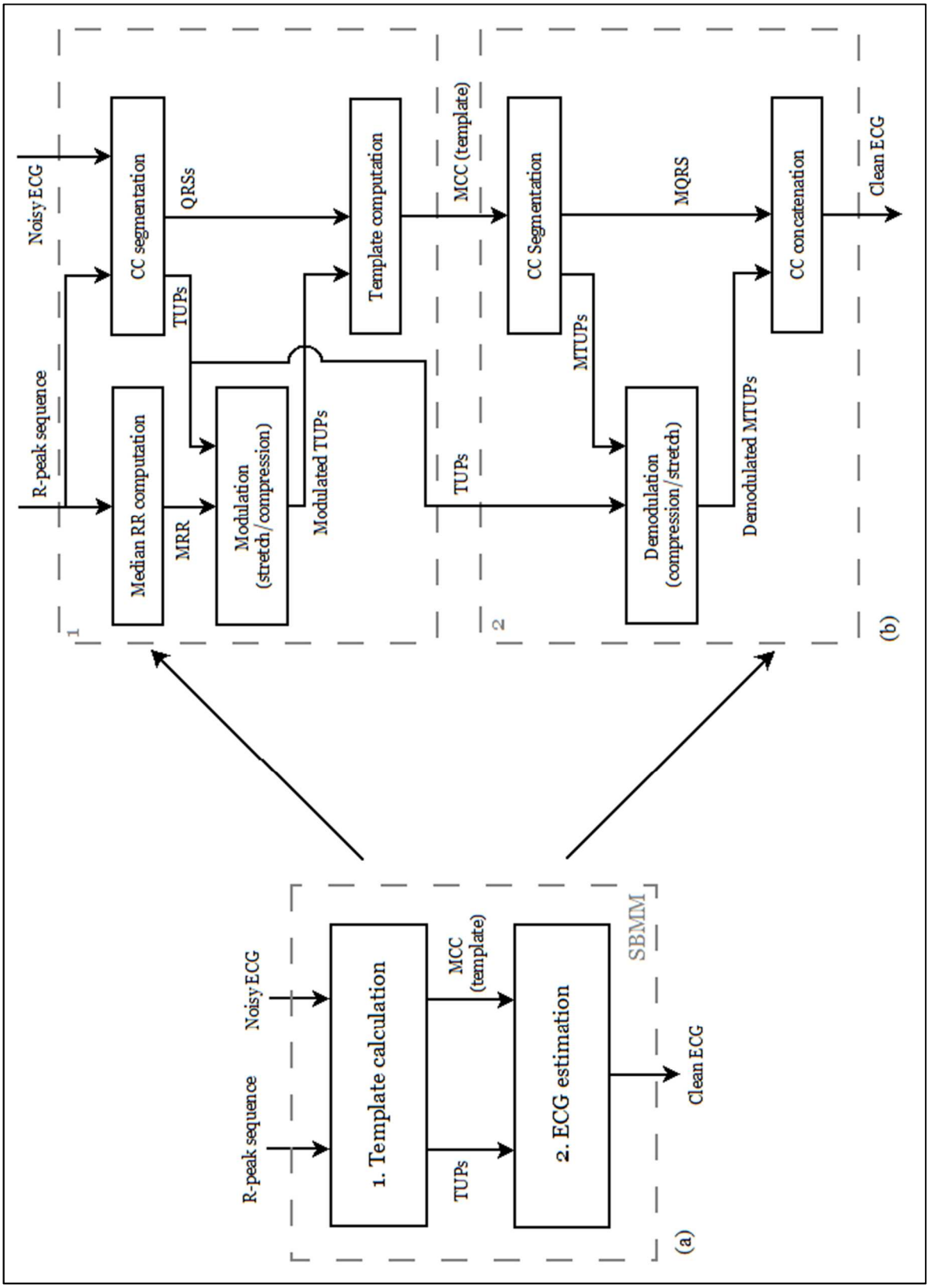

Fig. 3.2. *Block diagram of SBMM procedure in panel a, and of the two consecutive steps (template computation and ECG estimation,) of which it consists in panel b. [8]*

The autonomic nervous system is the main architect of this physiological variability. Indeed, autonomic nervous system controls the cardiac activity (constantly and unconsciously) in order to optimize blood circulation to the current physiological and emotional conditions of the subject. Other causes of ECG variability can be found in respiration, involuntary movements and non-physiological sources of noise, such as baseline wander (BW), electrode motion artifact (EMA), muscular artifact (MA) and power-line interference (PI). Particularly, BW can be caused by respiration and perspiration [102], EMA results from unexpected motion of the electrodes [103], MA is caused by the random contraction of muscle or sudden body movements [104], and PI is caused by radiation from high-voltage power lines (50 Hz) [105]. Sometimes, BW, EMA and MA are seen as baseline-related noise with different bandwidths [106]. The clinical utility of ECG signal may be jeopardized if the signal is corrupted by high levels of noise. Typically, ECG is pre-filtered by application of traditional linear filtering. However, this pre-filtering is not able to eliminate the noise frequency components within the ECG frequency band. If these noise components are heavily present, they may prevent a correct signal analysis unless further processing techniques are applied [102,103]. Template-based techniques [106] are often used to estimate ECG from the noisy recording when the signal is corrupted by noise that survived to the pre-filtering and R peaks are still detectable. The most of template-based techniques is not able to reproduce the physiological ECG variability that provides clinically useful information. In [8], SBMM is proposed as a template-based filtering procedure able to overcome this limit by adaptively adjustment of each reconstructed beat to the original beat morphology and duration. Also, always in [8], it has been demonstrated the robustness to noise of SBMM in comparison to another template-based technique present in the literature and the so called Standard Template Method (STM). In the following, the systematic study reported in [8] is described in detail.

Validation studies: simulation and clinical study

STM (which represents an adaptation of the method described in the literature [107]) and SBMM were used to estimate clean ECG signal from simulated signals and real recordings affected by various types and levels of noise [8].

The simulation study has the aim to evaluate the correctness of STM and SBMM Matlab implementations, and to test the ability of these procedures to estimate clean ECG tracings from recordings not corrupted by noise (ideal conditions). Simulated ECG tracing (6

signals) were created by using Matlab ECG simulator (http://www.mathworks.com/matlabcentral/fileexchange/ 10858- ecg- simulation- using-matlab). Each signal was 60 s long and characterized by a median HR of 75 bpm. Thus, median CC duration (MRR) was 800 ms. HRV was simulated by randomly selecting each CC duration within MRR ± P% • MRR range, with P%=0% (no HRV), 2.5%, 5%, 7.5%, 10% and 12.5%, respectively. ECG waveform amplitudes were: P: 0.20 mV; Q: −0.15 mV; R: 1.6 mV; S: −0.25 mV; and T: 0.40 mV. The duration of QRS segment was fixed constant at 100 ms, whereas the duration of T wave and P wave were, on average, 180 ms and 90 ms. In addition, for each beat, the latter values proportionally (linearly) vary in comparison to the preceding RR interval.

The clinical study has the aim to test SBMM ability to estimate clean ECG tracings from real recordings that are corrupted by various types and levels of noise, and to compare its performance against STM. Real ECG signals have been considered, all available at the PhysioBank of Physionet (www. physionet.org). Particularly, real ECG signals (18 two-lead) belong to the "MIT-BIH Normal Sinus Rhythm Database", and are recorded on healthy subjects with no arrhythmias [108]. All ECG signals were 60 s long and were characterized by HR ranging from 63 bpm to 110 bmp and HRV (measured as RR-interval standard deviation) ranging from 15 ms to 78 ms. All tracings were of good quality and the little portion of noise, which is present because the signals are real, was minimized by pre-filtering (0.5–35 Hz band-pass filtering and baseline subtraction by a 3^{rd}-order spline interpolation) and each was considered as reference. In addition, real noise recordings containing BW, EMA and MA (available at the "MIT-BIH Noise Stress Test Database" [108]) and simulated PI (sinusoid at 50 Hz) were considered. Then, these four-different kinds of noise were added to each reference ECG. Also, various levels of noise were considered: each noise tracing was multiplied for a gain factor ranging from 0 (no noise) to 1 with increments of 0.25. Fig. 3.3 reports an example of the noisy waveforms as function of noise level. STM and SBMM were applied to all real ECG tracings with added noise. An example of a real ECG tracing affected by various noise types (BW, EMA, MA and PI) and levels (gain factor from 0 to 1) is depicted in Fig. 3.4. STM and SBMM goodness to estimate a clean ECG tracing from a noisy recording was evaluated by comparing estimated with reference ECG tracings. Reference ECG tracings are designated by simulated ECG signals for simulation study and pre-filtered ECG signals for clinical study. Even if STM algorithm does not include the segmentation of CC, such

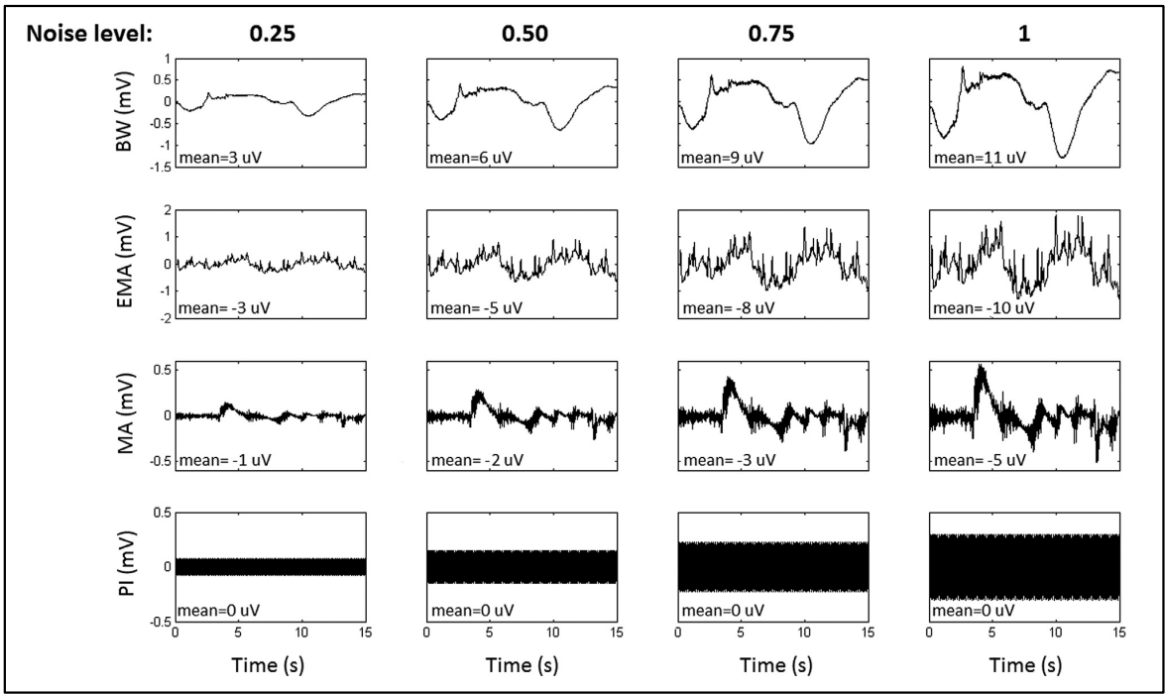

***Fig. 3.3**. BW, EMA, MA and PI waveforms and the corresponding mean values [8].*

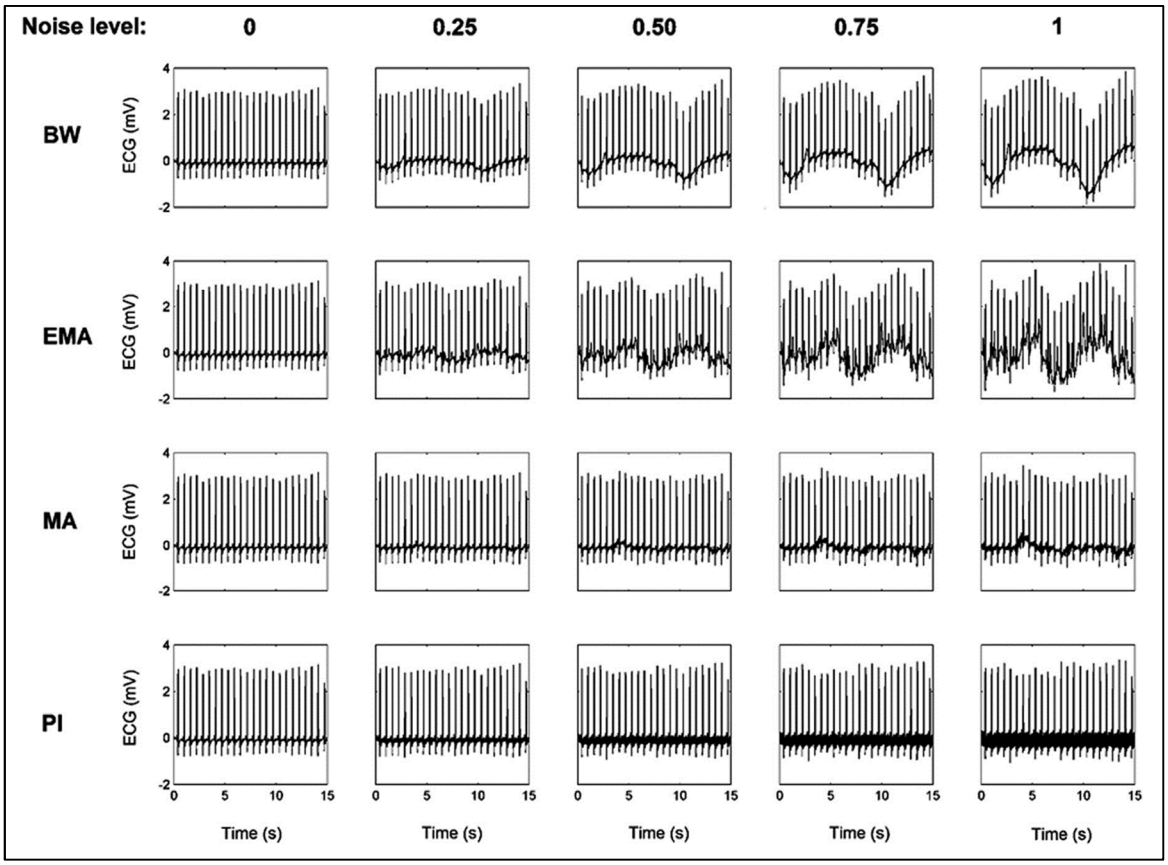

***Fig. 3.4.** Example of clinical ECG affected by BW, EMA, MA and PI noise, and levels (gain factor from 0 to 1) [8].*

segmentation is still performed also in STM in order to make possible the comparison between STM and SBMM. Then, two different errors were calculated, εQRS and εTUP, respectively relative to QRS and TUP segments and that follow the subsequent equations:

$$\varepsilon QRS_l = mean(max(|estQRS_l\,(n,i) - QRS_l(n,i)|)|_{i=1,2,\ldots,S_{QRS}})\Big|_{n=1,2,\ldots,N} \quad (3.1)$$

$$\varepsilon TUP_l = mean(max(|estTUP_l\,(n,i) - TUP_l(n,i)|)|_{i=1,2,\ldots,S_{TUP}})\Big|_{n=1,2,\ldots,N} \quad (3.2)$$

εQRS_l and εTUP_l (μV) for a specific lead l (simulation study:1lead, I; clinical study: 2 leads, I and II) correspond to the mean (over the N beats) of the maximum errors (along the S_{QRS} and S_{TUP} samples) between the estimated ($estQRS_l$ and $estTUP_l$) and reference (QRS_l and TUP_l) ECG amplitude in correspondence to QRS and TUP segment. Eventually, εQRS_l and εTUP_l were averaged over the leads in order to provide a single value of QRS error (εQRS) and TUP error (εQRS). Comparison between STM and SBMM was accomplished by computing the differences in the errors obtained by using the different procedures, as in the following equations:

$$dQRS = \varepsilon QRS|_{STM} - \varepsilon QRS|_{SBMM} \quad (3.3)$$

$$dTUP = \varepsilon TUP|_{STM} - \varepsilon TUP|_{SBMM} \quad (3.4)$$

Thus, when the values of dQRS and dTUP are greater than zero, these indicate respectively a better QRS and TUP estimation by SBMM than STM. εQRS and εTUP normality was evaluated by Lilliefors' test. However, not normal distributions were reported in terms of 50^{th} (median) [25^{th}–75^{th}] percentiles and compared using the Wilcoxon Rank-Sum test for equal median. Eventually, associations between parameters were evaluated using the Pearson's correlation coefficient (ρ). Statistical significance level (P) was set at 0.05.

Analysis of the results in simulation and clinical study

In simulation study, the application of STM to 6 simulated tracings provided the following results: εQRS=0 μV in all cases and εTUP = 0 μV, 56 μV, 91 μV, 117 μV, 151 μV and 189 μV for P% equal to 0%, 2.5%, 5%, 7.5%, 10% and 12.5%, respectively. Thus, εTUP was linearly increasing with P% (ρ=0.99, $P<10^{-4}$), which is HRV. Instead, the application of

SBMM to the same 6 simulated tracings provide the following results: εQRS=0 μV and εTUP=0 μVin all cases.

In clinical study, application of STM and SBMM in absence of noise provides estimations errors always greater than zero. Particularly, εTUP values were significantly lower than εQRS values (STM: 125 μV vs. 288 μV, $P<10^{-3}$; SBMM: 88 μV vs. 228 μV, $P<10^{-3}$; as reported in Table 3.1). εTUP values, but also εQRS values, tended to increase with HRV more markedly by using STM (εTUP: ρ=0.21; εQRS: ρ=0.45; Fig. 3.5) than SBMM (εTUP: ρ=0.02; εQRS: ρ=0.12, Fig. 3.5). Moreover, compared to STM, SBMM provided better ECG estimation, mainly in TUP segment (dTUP=35 μV, P<0.05; as reported in Table 3.2). Instead, in presence of noise and particularly in presence of BW, STM and SBMM provided εQRS and εTUP values statistically comparable with those obtained without noise, independently of noise level (as it can be seen in Table 3.1). Particularly, both methods provided εTUP values always significantly lower than εQRS values (STM: 103-141 μV vs. 240-245 μV, P<0.05; SBMM: 70-104 μV vs. 177-191 μV, P<0.05; as reported in Table 3.1). Usually, errors provided by using SBMM were lower than the corresponding errors provided by using STM. Consequently, dQRS and dTUP were greater than zero, but only a level of BW reached statistical significance (BW level: 0.5, dTUP=25 μV, P<0.05; Table 3.2). In presence of EMA, εQRS and εTUP values varied with noise level. Particularly, εQRS values provided by STM were increasing with EMA level (from 272 μV to 496 μV) and became significantly greater than εQRS calculated in absence of noise for EMA levels equal to 0.75 and 1 (394 μV and 496 μV, respectively, vs. 288 μV, P<0.05, Table 3.1). Instead, εQRS values provided by SBMM did not significantly increase with EMA level. Relatively to εTUP, both STM and SBMM provides such errors that increased with increasing of EMA level, and were always significantly higher than corresponding errors measured in the absence of noise (STM: 281–1056 μV vs. 125 μV, $P<10^{-3}$; SBMM: 154–499 μV vs. 88 μV, P<0.05, Table 3.1). EMA levels greater than or equal to 0.5, both STM and SBMM provide εTUP values significantly higher than εQRS values (STM: 545–1056 μVvs. 315–496 μV, P<0.05; SBMM: 257–499 μV vs. 176–232 μV, P<0.05, Table 3.1). Typically, SBMM provided smaller estimation errors than STM (Table 3.1). SBMM performed estimations significantly better for EMA levels greater than or equal to 0.5 in QRS segment (dQRS: 115–238 μV, $P<10^{-3}$, Table 3.2) and for any EMA level in TUP segment (dTUP: 123–464 μV, $P<10^{-3}$; Table 3.2). In presence of MA, STM provided significantly higher εTUP values than without noise for MA levels greater than or

Table 3.1. *ECG estimation errors by STM e SBMM in correspondence of the QRS and TUP segments as functions of noise kind and level [8].*

Types of noise	Noise level	**STM**		**SBMM**	
		εQRS (μV)	εTUP (μV)	εQRS (μV)	εTUP (μV)
None	0	288 [170;460]	125^{oo} [100;160]	228 [185;404]	88^{oo} [65;148]
BW	0.25	241 [150;315]	103^{oo} [77;149]	191 [136;352]	87^{oo} [51;170]
	0.5	240 [151;353]	133^{oo} [99;150]	185 [128;360]	79^{o} [53;176]
	0.75	242 [154;354]	141^{o} [96;194]	177 [119;361]	90^{o} [63;182]
	1	245 [154;353]	140^{o} [103;193]	184 [115;334]	104^{o} [68;191]
EMA	0.25	272 [180;336]	281^{**} [202;364]	188 [151;323]	$154^{*,§§}$ [115;234]
	0.5	315 [268;444]	$545^{**,o}$ [376;716]	176 [155;316]	$257^{**,§§,o}$ [230;365]
	0.75	394^{*} [341;531]	$799^{**,oo}$ [557;1069]	$217^{§}$ [178;357]	$379^{**,§§,oo}$ [304;486]
	1	496^{*} [379;617]	$1056^{**,oo}$ [755;1425]	$232^{§§}$ [178;361]	$499^{**,§§,oo}$ [396;630]
MA	0.25	221 [160;289]	93^{oo} [81;134]	187 [135;349]	88^{oo} [56;153]
	0.5	218 [170;297]	129^{oo} [105;158]	195 [138;345]	92^{oo} [61;145]
	0.75	215 [177;296]	$159^{*,o}$ [140;190]	178^{*} [146;299]	$91^{§,o}$ [68;143]
	1	241 [200;300]	$197^{*,o}$ [183;242]	184 [154;331]	$94^{§§,o}$ [75;134]
PI	0.25	235 [150;301]	98^{oo} [66;147]	192 [142;348]	89^{oo} [55;155]
	0.5	235 [149;300]	98^{oo} [66;147]	192 [142;349]	88^{oo} [54;156]
	0.75	235 [149;300]	98^{oo} [66;147]	192 [142;349]	86^{oo} [54;155]
	1	235 [148;300]	98^{oo} [66;147]	192 [143;349]	87^{oo} [54;155]

,:P<0.05, $P<10^{-3}$ when comparing corresponding errors obtained in the presence of noise vs.. no noise.*

§, §§: P<0.05, $P<10^{-3}$ when comparing corresponding errors by STM vs. SBMM.

o, oo: P<0.05, $P<10^{-3}$ when QRS vs. TUP errors by the same method.

equal to 0.75 (159–197 μV vs. 125 μV, P<0.05; Table 3.1). Instead, SBMM provided εQRS and εTUP values that were never significantly greater than values measured in absence of noise. STM and SBMM provided εQRS values significantly greater than corresponding εTUP values (STM: 221–241 μV vs. 93–197 μV, P<0.05; SBMM: 187–184 μV vs. 88–94 μV, P<0.05; Table 3.1). Generally, SBMM performed better than STM especially in TUP segments for MA levels greater than or equal to 0.5 (dTUP: 32–97 μV, P<0.05; Table 3.2). In presence of PI, STM and SBMM provided εQRS and εTUP values statistically comparable with those obtained without noise, independently of noise level (see Table 3.1). In addition, each method provided εTUP values always significantly lower than εQRS (STM: 98 μV vs. 235 μV, P<10^{-3}; SBMM: 86–89 μV vs. 192 μV, P<10^{-3}; Table 3.1). Also, εQRS and εTUP values provided by one method were not significantly different from those provided by the other (Tables 3.1 and 3.2).

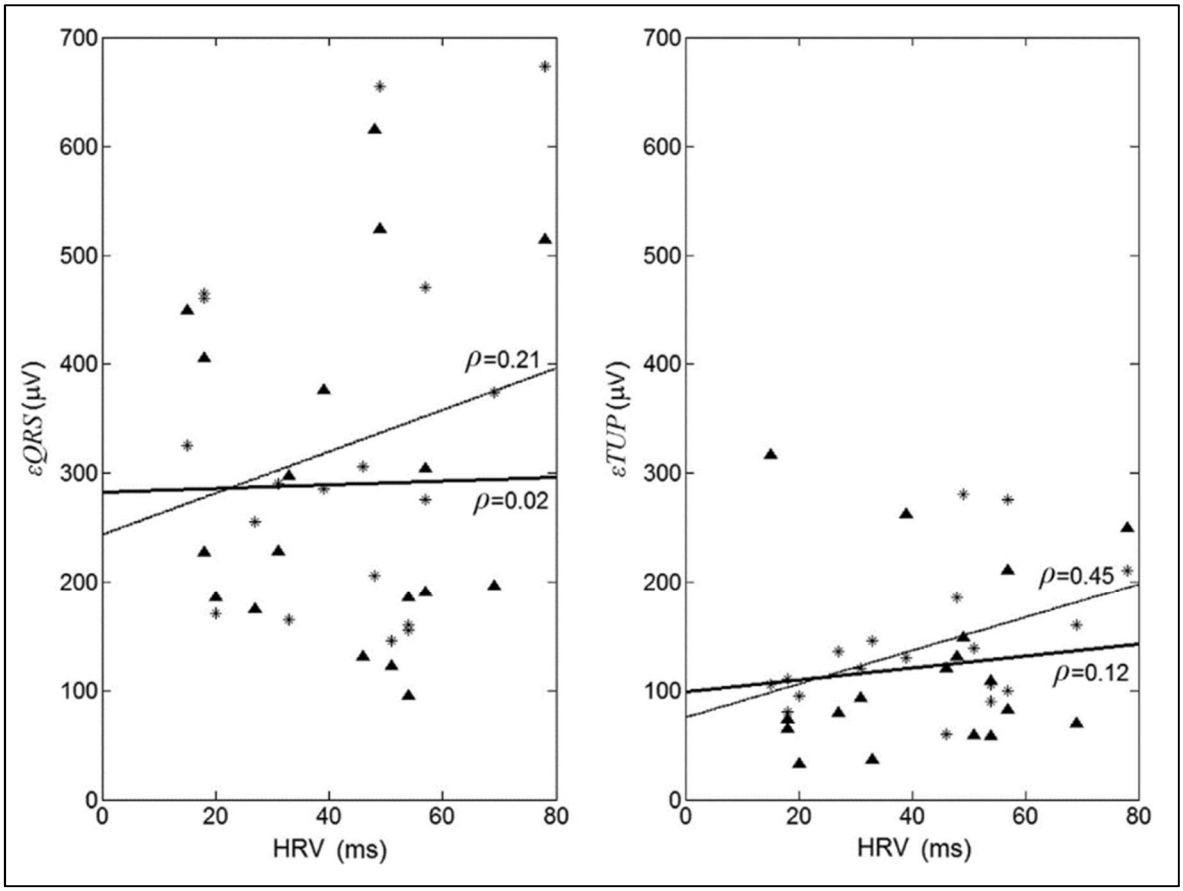

Fig. 3.5. *Association between QRS (εQRS; left panel) and TUP (εTUP; right panel) estimation errors by SBMM (▲) and STM (∗), and HRV (measured as RR-interval standard deviation), with relative regression lines (bold for SBMM and solid for STM) [8].*

Discussion of the obtained results

The study, reported in [8], represents the first systematic study that evaluates the SBMM procedure in comparison with another template-based technique present in literature, STM. Preliminary insights on SBMM have also been previously reported in [9-11].

Table 3.2. *Differences in the errors by STM and SBMM in correspondence of QRS and TUP segments [8].*

Types of noise	Noise level	dQRS (μV)	dTUP (μV)
None	0	64 [-30;159]	35* [-3;65]
BW	0.25	-10 [-136;70]	27 [-37;54]
	0.5	21 [-134;69]	25* [-18;75]
	0.75	36 [-123;125]	28 [-28;80]
	1	34 [-46;144]	44 [-16;77]
EMA	0.25	21 [-11;174]	123*** [33;148]
	0.5	115*** [30;194]	233*** [146;449]
	0.75	173*** [72;247]	345*** [206;688]
	1	238*** [92;352]	464*** [267;926]
MA	0.25	9 [-129;94]	18 [-27;53]
	0.5	21 [-115;97]	32* [-3;66]
	0.75	52 [-43;119]	68** [16;98]
	1	72 [-118;136]	97*** [47;131]
PI	0.25	-1 [-117;74]	21 [-38;44]
	0.5	-1 [-118;73]	20 [-38;44]
	0.75	-2 [-118;73]	20 [-38;45]
	1	-3 [-119;73]	20 [-37;45]

,, ***:P<0.05, P<0.01, P<10^{-3} when testing the hypothesis of dQRS and dTUP distribution having median greater than zero.*

Differently from STM, SBMM requires segmentation of each CC in QRS and TUP segment. The modulation and demodulation procedures (performed by stretching and compressing of TUP segment) allow the better adaptation of each CC to its original duration, and make SBMM most robust to HRV. To emphasize such features, the study also considered the simulated signals that allow to evaluate the SBMM performances in ideal conditions (i.e. in absence of noise). Indeed, the simulation study confirmed the peculiarity of SBMM to reproduce physiological ECG variability, since clean ECG tracings with various levels of HRV were analyzed. Particularly, by considering that QRS segment has a fixed duration, both methods reported no errors in QRS segments estimation. Instead, by considering that TUP segment has a variable duration in relation to instantaneous HR of the preceding RR interval, SBMM estimated TUP segments perfectly, while STM reported errors directly proportional to HRV. It might be argued that, in simulation study, the optimal performance of SBMM is caused by the fact that TUP segment linearly varies with instant HR and not affected by noise (ideal conditions). In clinical recordings, such conditions are never perfectly satisfied because the signals are obtained from healthy subjects affected by various physiologic levels of HRV. Anyway, they were pre-filtered to minimize the noise, since they had to be used as reference against which to calculate the estimation errors. Indeed, if you have ECG recordings heavily affected by noise, which is not easily removable, it would be impossible to evaluate the performance of SBMM because original and clean waveforms would have been unknown. Thus, various levels of noise (common noise which affected real ECG signal, such as BW, EMA, MA and PI) were added to the pre-filtered ECG tracings. By applying SBMM to clinical recordings not affected by noise, it is possible to demonstrate that εQRS and εTUP were always greater than zero (Tables 3.1 and Table 3.2). This can occur because clinical ECG are never perfectly clean also after pre-filtering, and linear dependency of TUP-segment duration on instant HR is only a first approximation of a physiologic relationship. Results also indicate that εTUP tend to increase with HRV (as shown in Fig. 3.5), and this relationship is stronger by using STM than SBMM (ρ=0.45 vs. ρ=0.12) thanks to the stretching/compressing of the modulation/demodulation process that characterize the latter method. In presence of noise, SBMM provide estimated signals with errors in QRS and TUP segments lower to those obtained by applying STM for all types and levels of noise. Indeed, SBMM not only includes HRV-adjustment procedure (described above) for TUP segment (Fig. 3.2), but also optimization processes that are not included in STM. Generally, in comparison with

STM, SBMM provides estimation improvements that were statistically more significant in TUP segment, and tended to increase with noise level. In presence of BW, MA and PI, ECG tracings were accurately estimated independently by the noise level. Instead, in presence EMA, and particularly in presence of high levels of EMA, estimation errors in both segments increased significantly, especially by using STM. As also reported in [109, 110], EMA is the most difficult noise to filter out, even if SBMM provides significantly better results than STM. STM and SBMM provide εQRS usually greater than εTUP, since QRS segment is characterized by waveforms with a higher frequency component than those included in TUP segment. Results obtained in presence of noise indicate that the use of median for the template computation allows a good reduction of all kinds of noise (Table 3.1), even if not perfectly zero-mean (Fig. 3.4). Thus, in case of not perfectly zero-mean noises, goodness of filtering procedure decreased with increasing noise amplitude (Table 3.1). Instead, for perfectly zero-mean noises, such as PI, filtering goodness was completely independent of the noise level. STM and SBMM, examples of template-based techniques, can be applied only if the positions of R peaks are known. In the most clinical cases, this condition is easily satisfied. However, when QRS-complex amplitude is higher than noise, a specific algorithm (such as Pan-Tompkins's algorithm [90]) can be applied to detect R-peak positions. For example, this occurs in non-invasive fECG. In non-invasive fECG, acquired by applying electrodes on the maternal abdomen, maternal ECG is overlapped with the fetal components, and the former has an amplitude much higher (about 5 times) than the latter. Thus, by knowing R-peaks position and by applying template-based techniques, maternal ECG is estimated and then subtracted to the Non-invasive fECG. In cases in which R peaks are not directly derivable from the original noisy recording, R peaks have to be indirectly obtained by using another ECG channel.

The main limitation of SBMM, found so far, is that clinical ECG tracings from healthy subjects are characterized by sinus beats. If few ectopic beats are present, they will not appear in the estimated ECG since only one template for the most frequent beat kind is computed. Future research will focus on SBMM improving in order to provide accurate ECG estimations, starting from noisy recordings of patients with significant cardiac pathology.

Summarizing, in comparison with another template-based technique (STM), SBMM provides a better clean ECG estimation from noisy recordings, able also to reproduce the

physiological ECG variability. Improvements are due to segmentation of each cardiac beat in QRS and TUP segments, and subsequent modulation/demodulation process (which involving stretching and compression) on TUP segment in order to adaptively adjust each estimate beat to the original beat morphology and duration

.

Chapter 4

Application of the Segmented-Beat Modulation Method for fetal electrocardiogram extraction

In this chapter, SBMM is applied to fECG estimation from the abdominal recording. It has been demonstrated that SBMM is particularly useful for denoising the non-invasive fECG and may contribute to the spread of this noninvasive technique in the clinical practice. Also, an improved version of Pan-Tompkins' algorithm for fetal applications is applied on fECG in order to have a good accuracy of R-peak detection for HR evaluations and subsequent processing.

4.1 Fetal electrocardiogram extraction by Segmented-Beat Modulation Method with optimal R-peak detection

SBMM, recently proposed as template-based filtering procedure for ECG denoising [8-11], has theoretic principles that make it suitable for fECG applications [111]. Particularly, SBMM was applied to invasive and non-invasive fetal recordings simultaneously acquired from pregnant woman during labor. The clinical data consists of 5 records, each includes 60 s long recordings from 5 different pregnant women during labor (which occurred within the 38^{th} - 41^{st} week of gestation), acquired in the Department of Obstetrics at the Medical University of Silesia. The acquisitions were accomplished by means of KOMPOREL system (sampling rate: 1000 Hz; resolution:16 bits) developed by ITAM Institute (Zabrze, Poland). Each record was constituted by invasive (or direct) recording (DREC) and a 4-channel non-invasive (or indirect) recording (IREC), simultaneously acquired. DREC was carried out with a spiral electrode on the fetal head. Instead, IREC was obtained by placing 4 electrodes around the navel, a reference electrode above the pubic symphysis and a common mode reference electrode (with active-

ground signal) on the left leg. All recordings are part of the "Abdominal and Direct Fetal Electrocardiogram Database" [91] of PhysioNet (www.physionet.org) [108], freely accessible on the web under the ODC Public Domain Dedication and License v1.0. The database has been fully anonymized and may be used without further Institutional Review Boards approval. Additional parameters, such as reference R-peak positions, are also available. R-wave locations were automatically determined in invasive fECG signal by means of on-line analysis applied in the KOMPOREL system. These locations were then verified (off-line) by a group of cardiologists, resulting in a set of reference markers precisely indicating R-wave locations. DREC is substantially a noisy version of direct fECG. Whereas IREC, besides indirect fECG, also contains maternal electrocardiogram (MECG) and other noise kinds. Thus, DREC and IREC can be mathematically modeled as follows:

$$DREC = DFECG + DN \tag{4.1}$$

$$IREC = IFECG + IN \tag{4.2}$$

where DFECG and IFECG represent the direct and indirect fECG signals, respectively; while DN e IN are the noise components affecting DREC and IREC, respectively. DFECG and IFECG were extracted from DREC and IREC, respectively, by application of SBMM, as depicted in Fig. 4.1. As previously said, SBMM is a denoising procedure for ECG signals that works under the hypothesis of knowing R-peak positions [8-11]. Particularly, DFECG extraction from DREC is depicted in Fig. 4.1, panel a. Thus, reference fetal R-peak positions and DREC were submitted to SBMM, which provides DFECG as output. DN was obtained by subtracting DFECG from DREC. Also, SBMM was applied to extract IFECG signal from each IREC channel (as shown in Fig. 4.1, panel b). Maternal ECG is the highest component in IREC, and maternal R-peaks were obtained by applying Pan-Tompkins' algorithm [94] to IREC. Thus, maternal R-peak positions and IREC were submitted to SBMM in order to get the maternal ECG (MECG). Successively, MECG was subtracted from IREC to obtain a noisy version of IFECG (IFECG + IN), that is, together with the fetal R-peak positions (the same used for DFECG extraction), was submitted to SBMM. Eventually, SBMM provided IFECG as output, and IN was obtained by

subtraction. Usually, SNR is used to relatively quantify the level of noise affecting a signal. In the following, it will explain the computation of SNR, which characterized fECG.

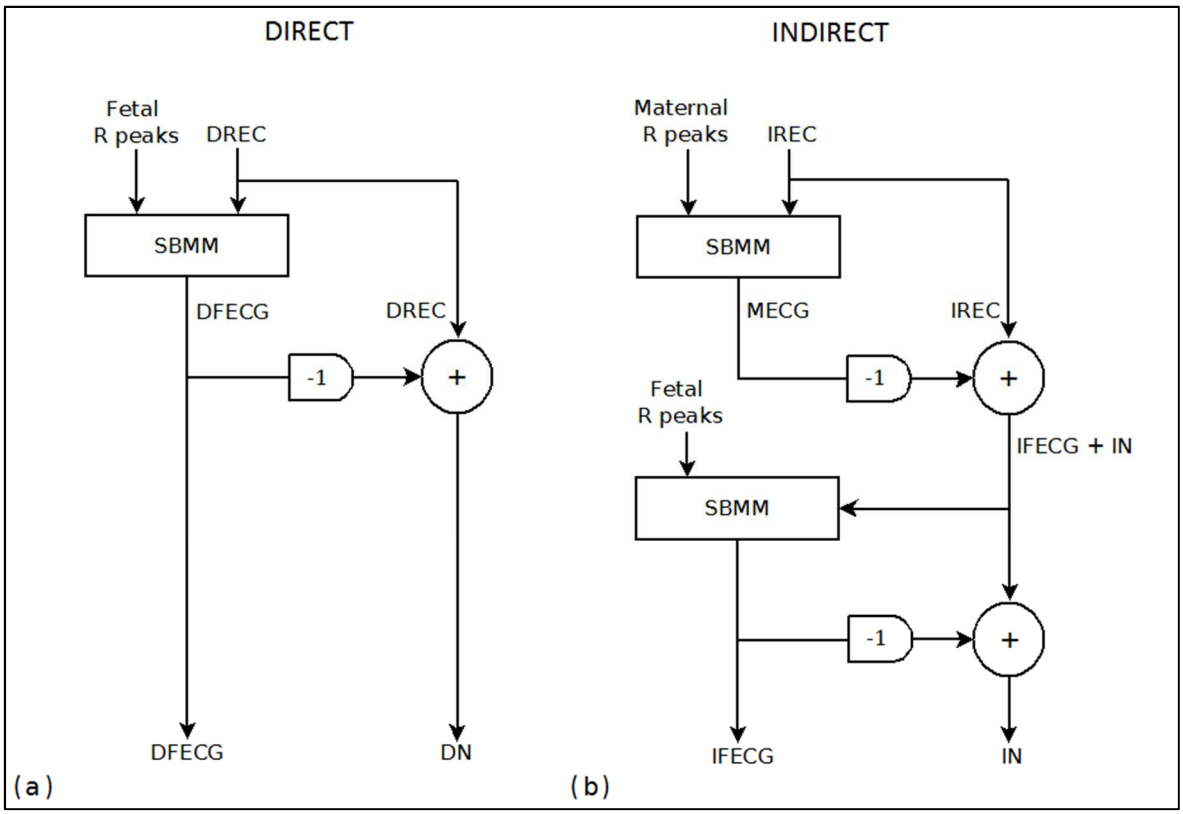

Fig. 4.1. *Block diagram of the procedure to extract DFECG and IFECG from DREC (panel a) and from a single channel of IREC (panel b), respectively, by means of SBMM [111].*

Signal-to-noise ratio computation for fetal electrocardiogram

SNR is typically expressed in decibel (dB) [112], and it may be obtained as the ratio between the signal amplitude over the noise amplitude. In this specific case, the signals of interest were DFECG and IFECG affected by the noise component, DN and IN respectively. Thus, direct SNR (DSNR) and indirect SNR (ISNR) can be obtained by the following equations:

$$DSNR = 20log_{10}\frac{DFECG\ amplitude}{DN\ amplitude} \qquad (4.3)$$

$$ISNR = 20log_{10}\frac{IFECG\ amplitude}{IN\ amplitude} \quad (4.4)$$

DFECG and IFECG can be considered as deterministic (pseudo-periodic) signals and thus, their amplitudes were computed as mean of the maximum-minus-minimum values over the beats. Instead, DN and IN are close to stochastic signals, and their amplitudes were computed as 4 times standard deviation. All amplitude values were computed over the 60 s of considered length of records. Particularly, ISNR was computed twice: once after MECG subtraction from IREC (ISNR1) and one after IFECG denoising (ISNR2), as shown in Fig. 4.1. Thus, ISNR2 describes the quality of the final IFECG tracing obtained from IREC using the SBMM [111].

Distributions of DFECG amplitude, IFECG amplitude, DN amplitude, IN amplitude, DSNR and ISNR were described in terms of median (50^{th}) [25^{th};75^{th}] percentiles and were compared using Wilcoxon Rank-Sum test for equal medians. Association between DFECG and IFECG (two different representations of the same electrophysiologic phenomenon, i.e. the electrical activity of the fetal heart) was evaluated using Pearson's correlation coefficient (ρ). Statistical significance level P was set at 0.05 in all cases.

Results obtained by applying SBMM in invasive and non-invasive fetal electrocardiograms

By way of example, Fig. 4.2 shows the SBMM application to record 1. DREC and IREC (channel 1), simultaneously acquired, are represented together with all their components. As shown, DFECG amplitude was much higher than IFECG amplitude (104 μV vs 18 μV), whereas the difference between DN and IN amplitudes was less marked (34 μV vs 14 μV). Thus, DSNR was higher than ISNR1 (9.8 dB vs 2.0 dB). Instead, the noise level affecting IFECG at the end of the SBMM procedure was very low, so that DSNR was lower than ISNR2 (10 dB vs 22 dB). In general, for all records, DFECG amplitude was always higher than IFECG amplitude, independently of the channel (Table 4.1). Consequently, median (over the records) DFECG amplitude was significantly higher than median IFECG amplitude (104 [89;157] μV vs 22 [16;29] μV, $P=7.66\cdot10^{-4}$). Whereas, DN amplitude was higher or equal to IN amplitude (independently of the channel) in records 1, 4 and 5, comparable in record 3 and lower in record 2 (Table 4.1). Consequently, median DN and IN amplitudes were not significantly different (70 [39;78] μV vs 49 [25;77] μV, P=0.45). Specifically, for the invasive fashion, median DN amplitude and median IN amplitude were

not significantly different (70 [39;78] μV vs 49 [25;77] μV, P=0.45). Instead, for the non-invasive fashion, median IFECG amplitude was significantly lower than median IN amplitude ($P=1.90\cdot10^{-3}$). Thus, DSNR is almost always greater than ISNR1 in all channels of every record, except channels 1 and 2 of record 5 (Table 4.1). Consequently, median DSNR was significantly greater than median ISNR1 (7 [3.5;10] dB vs -5 [-15;1] dB, $P=3.40\cdot10^{-3}$). Eventually, at the output of SBMM, the noise level affecting IFECG is mostly

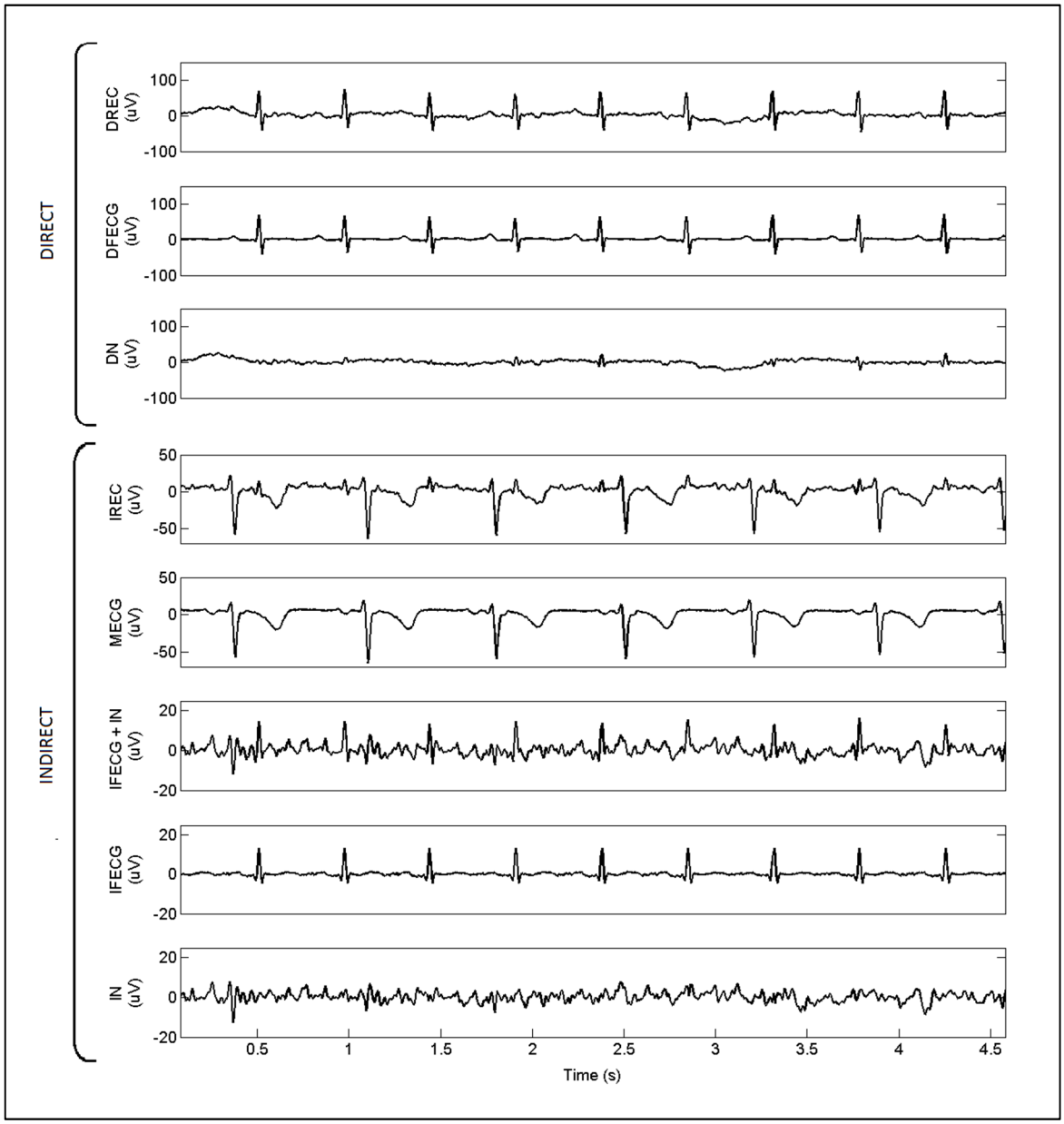

Fig. 4.2. *A segment (4.5 s) of DREC and IREC (record 1, channel 1), simultaneously acquired, together with all their components individually plotted (DFECG amplitude: 104 μV; DN amplitude: 34 μV; IFECG amplitude: 18 μV; and IN amplitude: 14 μV) [111].*

removed so that median DSNR was significantly lower than median ISNR2 (7 [3.5;10] dB vs 19 [16;22] dB, $P=9.00\cdot10^{-4}$). Correlation calculated between DFECG and IFECG was typically high and significant ($\rho=0.78$ [0.75;0.83], $P<10^{-208}$; Table 4.1). Only in records 3 and 5, ρ showed lower but still significant values ($\rho=0.45$ in channel 1 of record 3, and $\rho=0.28$ in channel 3 of record 5; $P<10^{-208}$) in correspondence of the channel with the lowest ISNR1 (-22 dB and -4 dB, respectively; Table 4.1). Also, Fig. 4.3 shows IREC channels (4) of record 5 after subtraction of MECG (i.e. IFECG+IN). Represented signals show a significant variability of amplitude among channels so that the IFECG component is more easily visible in some channels than in others. This can be generalized to all records (see Table 4.1). Indeed, ISNR1 variability among channels is a direct consequence of IFECG amplitude variability and IN amplitude variability.

Discussion of the obtained results

By the above-mentioned study, it is possible to evaluate the SBMM suitability for denoising of non-invasive fECG. Particularly, SBMM is used to denoise IREC in order to extract an IFECG of good quality at least comparable to that of DFECG, which is considered the gold standard for non-invasive fECG. Goodness of SBMM performance was assessed by correlating IFECG against DFECG. In future, a good correlation between IFECG and DFECG would justify the application of SBMM to IREC only. As previously said, SBMM works if R-peak positions are known. To avoid misplacements and ensure the correct localization of the fetal R peak, fetal R-peak detection was manually accomplished on DREC. R-peak detection must necessarily be automatic and not manual, and in real clinical cases, DREC and IREC are typically not simultaneously available. In order to evaluate the use of SBMM in real clinical conditions, it is important to observe that R-peak localization is quite straightforward from DREC where DFECG is the dominant component, whereas it may become very challenging from IREC [49,50] where, besides IFECG, are present other high amplitude components. Fetal R-peak localization is an interesting issue which, however, will be treated in the following.

According to results, DFECG amplitude was higher than IFECG amplitude (few hundred of μV the former, and tens of μV the latter), whereas the noise level was very variable over the records but, on average, comparable between the two acquisition modalities (invasive and non-invasive). Thus, DSNR was usually higher than ISNR1 and this result matches the expectations. DFECG is acquired by using electrodes in touch with the fetus, and thus its amplitude is expected to be quite large and DN can be represented by fetal physiological

Table 4.1. *Characteristics of the signal components in direct and indirect fetal recordings [111].*

RCD	*DREC*			*IREC*					*ρ*
	DFECG ampl (μV)	*DN ampl (μV)*	*DSNR (dB)*	*ch*	*IFECG ampl (μV)*	*IN ampl (μV)*	*ISNR1 (dB)*	*ISNR2 (dB)*	
1	*104*	*34*	*10*	*1*	*18*	*14*	*2*	*22*	*0.85**
				2	*23*	*30*	*-2*	*19*	*0.79**
				3	*21*	*15*	*3*	*22*	*0.87**
				4	*35*	*34*	*0*	*22*	*0.89**
2	*87*	*41*	*7*	*1*	*5*	*72*	*-23*	*10*	*0.63**
				2	*20*	*106*	*-15*	*19*	*0.82**
				3	*13*	*94*	*-17*	*16*	*0.81**
				4	*20*	*114*	*-15*	*18*	*0.75**
3	*89*	*73*	*2*	*1*	*5*	*70*	*-22*	*12*	*0.45**
				2	*18*	*77*	*-13*	*16*	*0.77**
				3	*11*	*76*	*-17*	*16*	*0.75**
				4	*22*	*83*	*-12*	*19*	*0.80**
4	*208*	*70*	*10*	*1*	*24*	*56*	*-8*	*20*	*0.83**
				2	*29*	*55*	*-6*	*20*	*0.76**
				3	*25*	*31*	*-2*	*21*	*0.83**
				4	*43*	*43*	*0*	*22*	*0.87**
5	*140*	*94*	*4*	*1*	*54*	*26*	*6*	*23*	*0.77**
				2	*41*	*24*	*5*	*22*	*0.76**
				3	*10*	*16*	*-4*	*15*	*0.28**
				4	*28*	*19*	*3*	*19*	*0.59**

*: $P<10^{-208}$

signals different to fECG, such as fetal electroencephalography. Instead, IFECG is acquired by using electrodes positioned on the maternal abdomen, and thus not in touch with fetus. IFECG amplitude is expected to be quite low and IN (besides MECG) may incorporate both fetal and maternal physiological signals (such as fetal electroencephalography and maternal uterine contractions, etc.). Although the differences in terms of amplitude and levels of noise which affect the signals, DFECG and IFECG were strongly correlated (ρ=0.78). This strong relationship confirms that DFECG and IFECG are different representation of the same physiological phenomenon, such as the electrical activity of the fetal heart. Since the correlation is independent from signal amplitude, the variability of IFECG and IN amplitudes in several channels does not reflect in ρ values. In addition, ISNR2 was lower than DSNR. This indicate that IFECG extracted by SBMM was characterized by a better signal quality than DFECG. When it evaluates SBMM applicability as denoising technique for fECG extraction, it is possible to consider 60 s long recordings. For monitoring of fetal parameters during labor, you should

consider longer recordings, since fetal parameters can last for hours. In these studies, 60 s windows of fECG should be iteratively filtered by SBMM in order to obtain clean fECG tracings from which to perform the measurements. Iterative application of SBMM allows almost real-time (about one-minute delay) evaluations of such parameters and adaptation to the physiological variability of fECG. The small number of signals considered is a possible limitation of this study. This is due to the fact that simultaneously recorded DREC and IREC are very rare. Nevertheless, the ρ values were statistically very significant in all

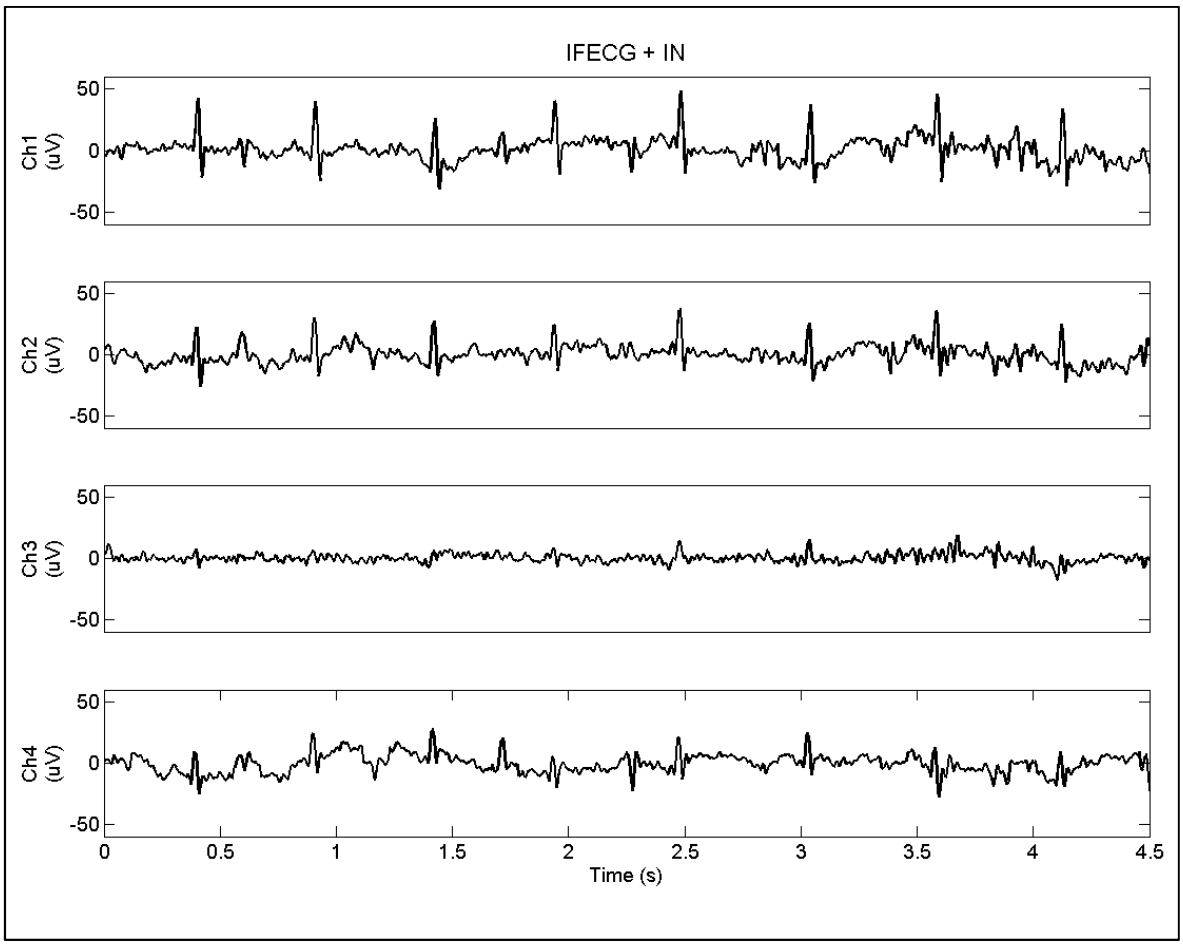

Fig. 4.3. *Representation of 4.5 s of 4 IREC channels (Ch) of record 5 after subtraction of MECG [111].*

cases ($P<10^{-208}$), so that SBMM ability to correctly extract fECG from both DREC and IREC was clearly demonstrated in spite of the limited number of application cases. Only occasionally lower values of ρ were observed. These may indicate that electrodes have not correctly acquired the signal or that the transformation from DFECG to IFECG might not

be perfectly linear, as assumed when computing ρ. This latter hypothesis is physiologically sustainable, since there is no determined geometrical relationship among the locations of the electrodes and of the fetal heart.

Summarizing, high correlation observed between DFECG and IFECG indicates that these signals have equivalent morphological content, and the finding that ISNR2 was higher than DSNR indicates that IFECG has better quality than DFECG. Thus, SBMM can be used to obtain clean and potentially clinically useful IFECG, also when DFECG is not available. SBMM application to IFECG may contribute to the spread of this technique in the clinical practice, since able to provide good quality fetal tracings in a noninvasive, safe, simple and economic way. At this time, the study [111] above mentioned was submitted at "The Open Biomedical Engineering Journal".

4.2 Optimal fetal R-peak identification in non-invasive fetal electrocardiogram

Fetal R-peak detection, is an essential step for getting information about fetal HR (bpm) and for extracting a clean IFECG from abdominal recordings by template-based techniques [113], such as SBMM. Pan-Tompkins' algorithm (PTA) [94] is the popular and traditional method for R-peak detection, originally designed for adult applications. Some studies [114,115] suggested its use also for fetal applications without, however, considering an eventual its adaptation to the fetal conditions. Thus, this work evaluates the suitability of PTA to fECG applications [116], and proposes some adjustments and optimizations to improve fetal R-Peak detection from IFECG.

Clinical data consisted in 60 s windows of the 5 records (RCD1 to RCD5) obtained from pregnant women during labor (between 38th-and 41st week of gestation) and constituting the "Abdominal and Direct Fetal Electrocardiogram Database" [91] of PhysioNet (www.physionet.org) [108], the same considered in the previously study. Thus, the records were obtained by means of the KOMPOREL system (ITAM Institute, Zabrze, Poland) and were performed in the Department of Obstetrics at the Medical University of Silesia. Each record is constituted by direct recording obtained by positioning a spiral electrode on the fetal head, essentially representing DFECG, and 4 simultaneously-acquired channels of an indirect abdominal recording obtained by placing 4 electrodes on the maternal abdomen,

essentially representing 4 channels of IREC. SBMM [8-11] was applied to each IREC in order to get 4 IFECG (IFECG1 to IFECG4) signals. Generally, DFECG was affected by a lower level of noise (and thus by a higher SNR) than IFECG.

Pan-Tompkins algorithm

PTA was proposed in 1985 and is the most commonly used algorithm for R-peak detection. Major details of PTA may be found in [94]. Briefly, R-peaks detection is accomplished by various processing steps as shown in Fig. 4.4, including 5-15 Hz bandpass filtering; 25 ms differentiation; squaring operation; and 150 ms moving-window integration. Two sets of detection adaptive thresholds (Sf and Si) are used to confirm that fiducial points (i.e. local maximum) detected from filtered and integrated signals are actually R peaks. A fiducial point is detected as an R-peak if confirmed in both derived and integrated signals.

Improved Pan-Tompkins algorithm for fetal R-peak identification

PTA was originally designed for R-peak detection in adult ECG, and it is not optimized for fetal R-peak detection. Thus, an improved version of the algorithm, called Improved Fetal Pan-Tompkins Algorithm (IFPTA), is proposed. Now, this study was submitted at "The Open Biomedical Engineering Journal". Specifically, IFPTA represents a possible adaptation of PTA to fECG applications. IFPTA includes an adjustment of the PTA parameters to fetal cases and a corrector to minimize detection number of false-positive and false-negative, which may occur when very noisy recordings, as IFECG, are used. As previously said, the mechanical function of the fetal heart differs from the adult heart due to a different blood circulation in the prenatal period. Then, fetuses and adults are characterized by morphologically similar ECG signals that contain the same basic ECG waves, even if each fECG representation differs from the corresponding adult ECG representation [48]. From quantitative point of view, fECG and adult ECG have some important differences because the size of fetal heart is significantly smaller than the adult heart. At first, fetal HR (and thus fECG bandwidth) is almost twice the adult HR (and thus fECG bandwidth) [5]. Also, the amplitude of fetal QRS complex is significantly lower than the adult QRS complex and strongly depending on lead, gestational age, and fetus position [14]. These physiological features determine the numerical values of PTA parameters. Thus, such values would be adjusted to allow a better R-peak detection from adult to fetal applications. Substantially, IFPTA is equal to PTA (as shown in Fig.4.4) but bandpass filtering is set between 9 and 27 Hz and moving-window integration is performed over an

80 ms window [116]. Such values are obtained by considering mean fetal HR about 1.8 times mean adult HR.

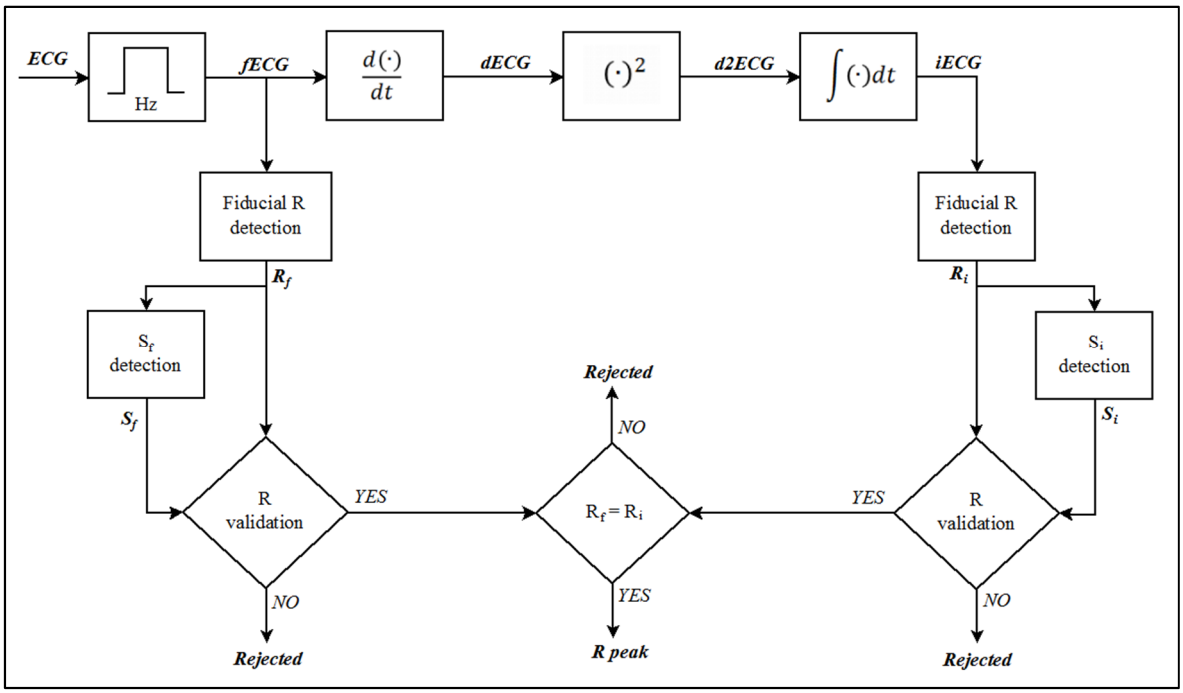

Fig. 4.4. *Block diagram of the Pan-Tompkins' (PTA) and improved fetal Pan-Tompkins' (IFPTA) algorithms for R-peak detection [116].*

In case of fECG tracings very corrupted by noise, a fetal R-peak corrector is applied in cascade to the main algorithm in order to improve the reliability of R-peak detection. The main algorithm provides R-peak sequence from which can be derived RR-interval sequence and the mean RR (MRR) is then computed. Also, each QRS complex is correlated against the mean QRS computed over the surrounding 9 beats. Corrector algorithm corrects beats characterized by low correlation, or surrounded by abnormally long or abnormally short RR intervals. Beats characterized by a low correlation (less than 0.70) preceded by a short RR interval (<0.90·MRR) and followed by a long RR interval (1.1·MRR), or preceded by a long RR interval and followed by a short RR interval, and probably identifies a couplet of false-positive/false-negative. Typically, this occurs when T wave is detected as R peak, and the following R peak is not detected because has a too short duration (less than refractory period). In this case, a beat is removed and another is

added. The added beat is positioned in the middle of the interval which is obtained by summing the two abnormal RR intervals. Then, its position is moved within a 0.15·MRR window and the position characterized by the best correlation is chosen. Correction is performed only if final correlation overcomes 0.70. Beat characterized by an RR interval > 1.4 MRR is a very long beat and it is identified false-negative beat. Insertion of additional beats is thus possibly required. The number of beats that should be added is given by rounding long RR interval over MRR. The position of each inserted R peak is moved within a 0.15·MRR window and, for each position, the correlation of the potential QRS complex with mean QRS is computed. The final position is chosen as the one with the highest correlation, which overcome 0.70 for a beat to be inserted. Eventually, beat characterized by RR interval (<0.50·MRR) is a very short interval and it is identified false- positive beats; removal of extra beats is thus possibly required. Of the two R peaks that identify RR, the one characterized by lowest correlation is removed. In any case, to be removed the correlation associated to R peak should be less than 0.8.

Signal characterization and statistics

In the same record, DFECG and IFECG were simultaneously acquired. Thus, R peak identified in one tracing is the same for the others. In this study, Physionet annotations were used as reference in order to evaluate PTA and IFPTA performances when applied to all DFECG and IFECG tracings. By KOMPOREL system, R-wave locations were automatically determined in the DFECG. Then, these locations were verified (off-line) by visual inspection by a group of cardiologists. The result is a set of reference markers that precisely indicate R-wave locations. R-peak sequence (manually or automatically obtained for each tracing) was used to compute HR and HRV. HR and HRV were expressed in terms of median value (50^{th}) and the difference between the 75^{th} and 25^{th} percentiles, calculated over the detected beats, in order to compensate possible errors in automatic detection that may introduce non-normal features in RR-interval distributions. Thus, false detection may cause errors (defined as absolute value between automatically measured HR minus manually determined HR) in HR and HRV. Moreover, it has been proposed a criterion for identifying the optimal IFECG channel for automatic R-peak detection as the one that show lower HRV. Automatic vs manual R-peak detections were compared. Instead, beats were classified as true positives, false positives, and false negatives in order to quantify R-peak detection accuracy by means of positive predictive value (PPV) and sensitivity (SE). PPV and SE follow the subsequent equations:

$$PPV = \frac{True\ positive}{True\ positive+False\ positive} \quad (4.5)$$

$$SE = \frac{True\ positive}{True\ positive+False\ negative} \quad (4.6)$$

Associations between SE vs SNR, PPV vs SNR and HRV vs SNR were evaluated using ρ and the regression line. Non-normal parameter distributions were described in terms of 50^{th} [25^{th};75^{th}] percentiles and comparted using Wilcoxon Rank-Sum test for equal medians.

Results obtained by applying PTA and IFPTA in invasive and non-invasive fetal electrocardiograms

Table 4.2 reported the results obtained by applying PTA and IFPTA in each DFECG and IFECG recording. As shown, IFPTA provided better results than PTA in all IFECG recordings, whereas performances of the two methods were comparable in DFECG. This occurred because SNR associated to DFECG is significantly greater than that associated to IFECG ([7 [3.5;10] dB vs -5 [-15;1] dB, $P=3.40\cdot10^{-3}$, as previously found in [111]). Particularly, HR and HRV errors calculated by PTA were significantly higher than those calculated by IFPTA (HR: 1.32 [1.00;2.74] bpm vs 0.00 [0.00;1.30] bpm, $P=4.22\cdot10^{-2}$; HRV: 37.26 [8.10;52.91] bpm vs 1.38 [0.00;4.70] bpm; $P=9.4\cdot10^{-4}$). Thus, PPV and SE associated to PTA were significantly lower than those associated to IFPTA (PPV: 0.60 [0.60;0.82] vs 0.90 [0.80;0.97], $P=1.04\cdot10^{-2}$; SE: 0.50 [0.34;0.84] vs 0.89 [0.72;0.96], $P=3.23\cdot10^{-2}$). In DFECG, R-peak detection was very accurate both by applying PTA and IFPTA (PPV and SE close to 1 in all cases, Table 4.2). Instead, in IFECG, performances of two methods were channel dependent (see Table 4.2). Particularly, PPV and SE are significantly correlated with SNR, which is channel dependent, both by using PTA and IFPTA (ρ= 0.75÷0.86, $P<10^{-4}$; Table 4.3). This indicates that in channels with higher SNR, R-peak detection is more accurate. However, SNR is inversely correlated with HRV, especially by using IFPTA ($|\rho|$= 0.45÷0.65, $P<10^{-2}$; Table 4.3). This indicates that when SNR decreases, HRV tends to increase. Consequently, PPV and SE significantly and inversely correlated with HRV both by using PTA and IFPTA ($|\rho|$=0.76÷0.91, P<10-4; Table 4.3). This indicates that in channels characterized by lower HRV, R-peak detection tends to be more accurate. This result is very important because in this way, it is possible

***Table 4.2**. Accuracy of automatic R-peak detection [116].*

			VI	PTA			IFPTA		
		SNR	**HR [HRV] (bpm)**	**HR [HRV] (bpm)**	**PPV**	**SE**	**HR [HRV] (bpm)**	**PPV**	**SE**
RCD 1	*DFECG*	*10*	*129.0 [2.8]*	*129.0 [2.8]*	*0.99*	*1.00*	*129.0 [2.8]*	*0.99*	*0.99*
	IFECG1	*2*		*141.2 [71.4]*	*0.46*	*0.50*	*129.0 [2.8]*	*0.88*	*0.88*
	IFECG2	*-2*		*157.9 [85.7]*	*0.38*	*0.45*	*129.0 [4.2]*	*0.85*	*0.86*
	IFECG3	*3*		*129.0 [21.8]*	*0.72*	*0.71*	*129.0 [3.9]*	*0.93*	*0.92*
	IFECG4	*0*		*129.0 [11.1]*	*0.79*	*0.80*	*129.0 [2.8]*	*0.95*	*0.95*
RCD 2	*DFECG*	*7*	*125.0 [4.0]*	*125.0 [3.6]*	*0.99*	*1.00*	*125.0 [4.0]*	*0.99*	*1.00*
	IFECG1	*-23*		*127.7 [65.2]*	*0.18*	*0.11*	*127.7 [51.4]*	*0.23*	*0.13*
	IFECG2	*-15*		*126.3 [46.7]*	*0.54*	*0.44*	*125.0 [6.6]*	*0.83*	*0.81*
	IFECG3	*-17*		*125.0 [35.7]*	*0.46*	*0.27*	*123.7 [27.9]*	*0.72*	*0.43*
	IFECG4	*-15*		*123.7 [42.8]*	*0.24*	*0.08*	*123.7 [37.8]*	*0.42*	*0.22*
RCD 3	*DFECG*	*2*	*127.7 [1.3]*	*127.7 [1.3]*	*1.00*	*1.00*	*127.7 [1.3]*	*1.00*	*1.00*
	IFECG1	*-22*		*125.0 [46.4]*	*0.25*	*0.15*	*123.7 [44.6]*	*0.19*	*0.09*
	IFECG2	*-13*		*127.7 [41.9]*	*0.58*	*0.46*	*127.7 [2.7]*	*0.89*	*0.89*
	IFECG3	*-17*		*127.7 [39.4]*	*0.57*	*0.42*	*126.3 [4.0]*	*0.82*	*0.69*
	IFECG4	*-12*		*127.7 [51.5]*	*0.61*	*0.49*	*127.7 [2.7]*	*0.90*	*0.86*
RCD 4	*DFECG*	*10*	*131.9 [11.4]*	*131.9 [11.4]*	*0.98*	*1.00*	*131.9 [11.4]*	*0.98*	*1.00*
	IFECG1	*-8*		*142.9 [90.4]*	*0.31*	*0.34*	*131.9 [19.2]*	*0.73*	*0.73*
	IFECG2	*-6*		*144.6 [100.1]*	*0.30*	*0.33*	*133.3 [15.8]*	*0.87*	*0.89*
	IFECG3	*-2*		*134.8 [31.4]*	*0.75*	*0.73*	*133.3 [14.5]*	*0.94*	*0.93*
	IFECG4	*0*		*133.3 [22.7]*	*0.81*	*0.83*	*133.3 [14.5]*	*0.94*	*0.95*
RCD 5	*DFECG*	*4*	*130.4 [8.3]*	*130.4 [9.0]*	*0.99*	*1.00*	*130.4 [9.0]*	*1.00*	*1.00*
	IFECG1	*6*		*131.9 [15.8]*	*0.84*	*0.88*	*130.4 [9.6]*	*0.97*	*0.96*
	IFECG2	*5*		*131.9 [21.0]*	*0.76*	*0.79*	*130.4 [8.3]*	*0.97*	*0.97*
	IFECG3	*-4*		*134.8 [88.3]*	*0.26*	*0.28*	*130.4 [13.9]*	*0.70*	*0.68*
	IFECG4	*3*		*131.9 [45.6]*	*0.60*	*0.61*	*130.4 [9.3]*	*0.95*	*0.94*

***Table 4.3.** Association between noise, HRV and accuracy of R-peak detection [116].*

	PTA		IFPTA	
	ρ	P	ρ	P
PPV vs SNR	*0.75*	$1.17 \cdot 10^{-5}$	*0.79*	$2.72 \cdot 10^{-6}$
SE vs SNR	*0.86*	$4.16 \cdot 10^{-8}$	*0.83*	$3.42 \cdot 10^{-7}$
SNR vs HRV	*-0.45*	$2.25 \cdot 10^{-2}$	*-0.65*	$4.86 \cdot 10^{-4}$
PPV vs HRV	*-0.86*	$3.28 \cdot 10^{-6}$	*-0.76*	$9.33 \cdot 10^{-6}$
SE vs HRV	*-0.91*	$3.76 \cdot 10^{-10}$	*-0.90*	$6.30 \cdot 10^{-10}$

to identify the optimal channel for R-peak detection. Then, according to this criterion, IFECG4 in RCD1, IFECG3 in RCD2, IFECG3 in RCD3, IFECG4 in RCD4, and IFECG1 in RCD5 are the optimal IFECG channels when using PTA. Whereas, IFECG4 in RCD1, IFECG2 in RCD2, IFECG4 in RCD3, IFECG4 in RCD4 and IFECG2 in RCD5 are the optimal channels when using IFPTA (Table 4.2). By using these optimal IFECG channels, accuracy of R-peak detection by IFPTA (PPV: 0.94 [0.88;0.96]; SE: 0.95 [0.85;0.96]) significantly overcomes the accuracy obtained by PTA (PPV: 0.79 [0.54;0.82], P= $2.38 \cdot 10^{-2}$; SE: 0.80 [0.38;0.84], P=$4.76 \cdot 10^{-2}$), and it approaches that of DFECG (PPV: 0.99 [0.98;1.0], P=$7.90 \cdot 10^{-3}$; SE:1.00 [1.00;1.00], P=$7.90 \cdot 10^{-3}$).

Discussion of the obtained results

Automatic R-peak detection is a fundamental step in the computerized analysis of fECG. However, R-peak detection in fECG may became very challenging, especially for IFECG that is corrupted by physiologic interferences and noise which may completely cover the fetal R peaks. PTA was originally designed to automatically detect R peaks in adult ECG. In this study, PTA is applied to fECG tracings and its accuracy in detecting R peaks was evaluated and compared with IFPTA. The latter is a PTA adaptation for fetal cases that includes some adjustments of PTA parameters and a corrector to minimize false detections. PTA and IFPTA were tested on the "Abdominal and Direct Fetal Electrocardiogram Database" [91] of PhysioNet [108], specifically used to test and evaluate automatic processing procedures on fECG [5,91]. Each record, contained in the database, includes DFECG (considered gold standard) and 4 channel IFECG, simultaneously acquired. Large IFECG databases are more easily available, such as for example "Non-Invasive Fetal Electrocardiogram Database" of Physionet [108] which includes 55 cases. Typically, these databases not include IFECG signals, and thus are more useful for clinical applications of already tested algorithms. Instead, database of only DFECG signals are rarer because to perform the invasive monitoring on low-risk women it could become not ethical. Although rather small, the number of considered signals (5 DFECG and 20 IFECG) was sufficient for evaluate PTA and IFPTA application to FECG [116]. Results indicate that both methods have an accuracy (quantified by PPV and SE) that increases with increasing of SNR; and for each tracing (and thus for each value of SNR), IFPTA provides better results than PTA. Both methods provide comparable results when applied to DFECG (with a higher SNR) thus indicating that PTA could be used in these recordings. Whereas, IFPTA provides a better accurate R-peak detection since the

difference between PTA and IFPTA was significant in IFECG tracings. Thus, PTA should not be used in IFECG applications, and IFPTA is preferable. Since SNR was channel-dependent (Table 4.2), also R-peak detection was channel-dependent. The channels were simultaneously acquired, and thus, only most accurate R-peak detection may be considered. Only if needed, R-peak detection can be performed on all channels. Since the accuracy increases with SNR, the better choice should be that to choose the lead characterized by the highest SNR. However, SNR may not be always available, and an accurate R-peak detection is needed for quantification of SNR [111]. Thus, SNR cannot be used to identify a priori the best channel for R-peak detection and an indirect SNR measure is desirable. HRV necessarily increase in presence of false-positive and false-negative. Therefore, HRV was used as an indirect measure of SNR. Indeed, HRV was found inversely correlated with the accuracy of R-peak detection, and IFPTA accuracy is always better than PTA accuracy for each HRV value. If it uses IFPTA in IFECG signals, by choosing the optimal channel as the one with the lowest HRV (always corresponding to highest PPV and SE), IFPTA accuracy was high (PPV=94%; SE=95%) and next to DFECG (PPV=99%, SE=100%). Thus, IFPTA represents a good tradeoff between the desire of using IFECG and the need of having a good R-peak detection for clinical evaluation on HR.

Summarizing, for fetal application where it uses IFECG, IFPTA is to be preferred over PTA because accuracy of R-peak detection is much higher. At this time, the study [116] above mentioned, was submitted at "The Open Biomedical Engineering Journal".

Conclusion

SBMM can be considered among the template-based filtering techniques. It performs an estimation of clean ECG signal from a noisy recording, and in comparison, to others template-based techniques, is able to preserve the physiological ECG variability of the original signal. This is due to segmentation of each cardiac beat in two segments (QRS and TUP), and subsequent modulation/demodulation process (which involving stretching and compression) on TUP segment for adaptive adjustment of each estimate beat to the original beat morphology and duration. In adult ECG applications, it has been demonstrated its better robustness to noise. In fECG applications, SBMM can be used to obtain clean and potentially clinically useful non-invasive fECG, also when invasive fECG is not available. Thus, SBMM may contribute to the spread of the non-invasive fECG in the clinical practice, since able to provide a good quality fECG in a noninvasive, safe, simple and economic way.

References

[1]. AA. Baschat. Integrated fetal testing in growth restriction: Combining multivessel Doppler and biophysical parameters. Ultrasound Obst Gyn 2003; 21:1–8.

[2]. C. Velayo, N. Sato, T. Ito, H. Chisaka, N. Yaegashi, K. Okamura, Y. Kimura. Understanding congenital heart defects through abdominal fetal electrocardiography: case reports and clinical. J. Obstet. Gynaecol. 2011; 37:428–435.

[3]. V. Regitz-Zagrosek, C. Blomstrom Lundqvist, C. Borghi, R. Cifkova, R. Ferreira, J-M. Foidart, J. S. R. Gibbs, C. Gohlke-Baerwolf, B. Gorenek, B. Iung, M. Kirby, A.H.E.M. Maas, J. Morais, P. Nihoyannopoulos, P.G. Pieper, P. Presbitero, J.W. Roos-Hesselink, M. Schaufelberger, U. Seeland, L. Torracca. ESC Guidelines on the management of cardiovascular diseases during pregnancy. The Task Force on the Management of Cardiovascular Diseases during Pregnancy of the European Society of Cardiology (ESC). Eur. Heart J. 2001; 32;3147–3197.

[4]. R. Goddard. Electronic fetal monitoring. Brit. Med. J. 2001; 322:1436–1437.

[5]. A. Agostinelli, M. Grillo, A. Biagini, C. Giuliani, L. Burattini,S. Fioretti, F. Di Nardo, S. R. Giannubilo, A. Ciavattini, L. Burattini. Non invasive fetal electrocardiography: An overview of the signal electrophysiological meaning, recording procedures, and processing techniques. Ann. Noninvasive Electrocardiol.2015; 20:303-313.

[6]. D. Gibb, S. Arulkumaran. Fetal monitoring in practice, Churchill Livingstone, 3rd edition, London, UK, 2008.

[7]. Y. Kimura, N. Sato, J. Sugawara, C. Velayo, T. Hoshiai, S. Nagase, T. Ito, Y. Onuma, A. Katsumata, K. Okamura, N. Yaegashi. Recent Advances in Fetal Electrocardiography. TOMDJ 2012; 4:7-12.

[8]. A. Agostinelli, A. Sbrollini, C. Giuliani, S. Fioretti, F. Di Nardo, L. Burattini, Segmented beat modulation method for electrocardiogram estimation from noisy recordings. Med Eng Phys 2016; 38:560-568.

[9]. A. Agostinelli, C. Giuliani, L. Burattini. Extracting a clean ECG from a noisy recording: a new method based on segmented-beat modulation. CinC 2014; 41:49-52.

[10]. A. Agostinelli, C. Giuliani, S. Fioretti, F. Di Nardo, L. Burattini. The segmented-beat modulation method for ECG estimation. IEEE EMBS 2015; 2856-2859.

[11]. A. Agostinelli, C. Giuliani, S. Fioretti, F. Di Nardo, L. Burattini. Robustness of the segmented-beat modulation method to noise. CinC 2015; 42:205-208.

[12]. L. Jana. Early Fetal Heart Development: 0-9 Weeks. The Dr. Spock Company 2004.

[13]. MC. Allen, PK. Donohue, AE. Dusman. The limit of viability – neonatal outcome of infants born at 22 to 25 weeks' gestation. Bull Soc Roy Belg Gynec Obstet Oct 1993; 329:1597–1601.

[14]. R. Sameni, G. Clifford. A review of fetal ECG signal processing; issues and promising directions. Electrophysiol Ther J 2010; 3:4–20.

[15]. T. Oostendorp, A. van Oosterom, H: Jongsma. Electrical properties of tissues involved in the conduction of fetal ECG. Biomed Eng Comput 1989; 27:322–324.

[16]. RA. Brace, EJ. Wolf. Normal amniotic fluid volume changes throughout pregnancy. Am J Obstet Gynecol 1989; 161:382–388.

[17]. EK. Osei, K. Faulkner. Fetal position and size data for dose estimation. Br J Radiol 1999; 72:363–370.

[18]. JB. Roche, EH. Hon. The fetal electrocardiogram. V. Comparison of lead systems. Am J Obstet Gynecol 1965; 92:1149–1159.

[19]. AC. Guyton, JE. Hall. Textbook of Medical Physiology. W.B. Saunders company, USA, 10th edition, 2000.

[20]. G. Mielke, N. Benda. Cardiac output and central distribution of blood flow in the human fetus. Circulation 2001; 103:1662–1668.

[21]. NP. De Pasquale, GE. Burch. The electrocardiogram, ventricular gradient and spatial vectorcardiogram during the first week of life. Am J Cardiol 1963; 12:482–493.

[22]. M. Artman, L. Mahony, DF. Teitel. Neonatal cardiology. McGraw-Hill companies, USA, 2002.

[23]. S. Yagel, NH. Silverman, U. Gembruch. Fetal cardiology: embryology, genetics, physiology, echocardiographic evaluation, diagnosis and perinatal management of cardiac diseases. Informa Healthcare Inc, USA, 2nd edition, 2009.

[24]. DB. Geselowitz. Dipole theory in electrocardiography. Am. J. Cardiol 1964; 14:301–306.

[25]. E. Frank. General theory of heart-vector projection. Circ Res 1954; 2:258–70.

[26]. HC. Burger, JB. Van Milaan. Heart-vector and leads. Br Heart J 1946; 8:157–161.

[27]. W. Einthoven. Weiteres ¨uber das elektrokardiogram. Pfl¨uger Arch ges Physiol 1908; 122:517–548.

[28]. T. Oostendorp. Modelling the foetal ECG. Phd thesis. Radboud universiteit. The Netherlands, 1989.

[29]. J. Malmivuo, R. Plonsey. Bioelectromagnetism - Principles and Applications of Bioelectric and Biomagnetic Fields, Oxford University Press, USA, 1995.

[30]. E. Frank. An accurate, clinically practical system for spatial vectorcardiography. Circulation 1956; 13:737–749.

[31]. R. Vullings. Non-invasive fetal electrocardiogram: Analysis and interpretation. PhD Thesis. Technische Universteit Eindhoven 2010.

[32]. LK. Hornberger, DJ. Sahn. Rhythm abnormalities of the fetus. Heart 2007; 93:1294–1300.

[33]. CS. Kleinman, RA. Nehgme. Cardiac arrhythmias in the human fetus. Pediatr Cardiol 2004; 25:234–251.

[34]. J. Spilka. Complex approach to fetal heart rate analysis: A hierarchical classification model. PhD thesis. Czech Technical University Prague 2013.

[35]. JP. Neilson. Fetal electrocardiogram (ECG) for fetal monitoring during labour. Cochrane Database Syst Rev 2013; 5:1–29.

[36]. E. Sadovsky, WZ. Polishuk. Fetal movements in utero nature, assessment, prognostic value, timing of delivery. Obstet Ginecol 1977; 50:49–55.

[37]. RK. Freeman, TJ. Garite, MP. Nageotte, LA. Miller. Fetal Heart Rate Monitoring, 4th edition, USA, 2012.

[38]. B. Gültekin-Zootzmann. The history of monitoring the human fetus. J. Perinat. Med 1975; 3:135-144.

[39]. E. Blix, O. Sviggum, K.S. Koss, P. Øian. Inter-observer variation in assessment of 845 labour admission tests: comparison between midwives and obstetricians in the clinical setting and two experts. BJOG 2003; 110:1-5.

[40]. KR. Greene, GS. Dawes, H. Lilja, KG. Ros´en. Changes in the ST waveform of the fetal lamb electrocardiogram with hypoxemia. Am J Obstet Gynecol 1982; 144:950–958.

[41]. H. Lilja, K. Karlsson, I. Kjellmer, K. Lindecrantz, T. Olsson, KG. Ros´en. Heart rate variability and electrocardiogram changes in the fetal lamb during hypoxia and beta-adrenoceptor stimulation. J Perinat Med 1984; 12:115–125.

[42]. KG. Ros´en, I. Kjellmer. Changes in fetal heart rate and ECG during hypoxia. Acta Physiol Scand 1975; 93:59–66.

[43]. KG. Ros´en, KH. H¨okeg°ard, I. Kjellmer. A study of the relationship between the electrocardiogram and hemodynamics in the fetal lamb during asphyxia. Acta Physiol Scand 1976; 98:275–284.

[44]. KG. Ros´en, A. Dagbjartsson, BA. Henriksson, H. Lagercrantz, I. Kjellmer. The relationship between circulating catecholamines and ST waveform in the fetal lamb electrocardiogram during hypoxia," Am J Obstet Gynecol 1984; 149:190–195.

[45]. I. Amer-W°ahlin, C. Hellsten, H. Nor´en, H. Hagberg, A. Herbst, I. Kjellmer, H. Lilja, C. Lindoff, M. M°ansson, L. M°artensson, P. Olofsson, A. Sundstr¨om, K. Mars´al. Cardiotocography only versus cardiotocography plus ST analysis of fetal electrocardiogram for intrapartum fetal monitoring: a Swedish randomised controlled trial. Lancet 2001; 18:534–538.

[46]. MEMH. Westerhuis, A. Kwee, AA. van Ginkel, AP. Drogtrop, WJA. Gyselaers, GHA. Visser. Limitations of ST analysis in clinical practice: three cases of intrapartum metabolic acidosis. BJOG 2007; 114:1194–1201.

[47]. HML. Jenkins. Thirty years of electronic intrapartum fetal heart rate monitoring: discussion paper. J Roy Soc Med 1989; 82:210-214.

[48]. M. Hasan, M. Reaz, M. Ibrahimy, M. Hussain, J. Uddin. Detection and Processing Techniques of FECG Signal for Fetal Monitoring. BPO 2009; 11:263-295.

[49]. S. Lee, J. Kruse. Biopotential Electrode Sensors in ECG/EEG/EMG Systems. www.analog.com/MedicalICs.

[50]. MR. Neuman. Biopotential electrodes. Med. Instrum. 2008; 5:189-240.

[51]. A. Gruetzmann, S. Hansen, J. Muller. Novel dry electrodes for ECG monitoring. Physiol Meas 2007; 8:1375-1390.

[52]. EC. Karvounis, MG. Tsipouras, DI. Fotiadis, KK. Naka. An Automated Methodology for Fetal Heart Rate Extraction from the Abdominal Electrocardiogram. IEEE T Inf Technol B 2007; 11:628-638.

[53]. M. Kotas, J. Jezewski, K. Horoba, A. Matonia. Application of spatio-temporal filtering to fetal electrocardiogram enhancement. Comput Meth Prog Bio 2011; 194:1-9.

[54]. M. Kotas, J. Jezewski, A. Matonia, T. Kupka. Towards noise immune detection of fetal QRS complexes. Comput Meth Prog Bio 2010; 97:241-256.

[55]. J. Tsao, CY. Hsu, MT. Lo. A Supervised ICA Algorithm for Fetal ECG Extraction. IEEE ISSPIT 2008; 327-330.

[56]. A. Matonia, J. Jezewski, K. Horoba, A. Gacek, P. Labaj. The maternal ECG suppression algorithm for efficient extraction of the fetal ECG from abdominal signal. IEEE EMBS 2006; 3106- 3109.

[57]. P. Bergveld, W.J.H. Meijer. A New Technique for the Suppression of the MECG. IEEE T. Bio-Med. Eng. 28 (1981) 348-354.

[58]. D. Marossero, T. Euliano, N. Euliano, J. Principe. Maternal-fetal monitoring system. Patent No: US 8,275,451 B2, 25; 2012.

[59]. SMM. Martens, C. Rabotti, M. Mischi, R. J. Sluijter. A robust fetal ECG detection method for abdominal recordings. Physiol Meas 2007; 28:373–388.

[60]. G. Clifford, R. Sameni, J. Ward, J. Robinson, A. J. Wolfberg. Clinically accurate fetal ECG parameters acquired from maternal abdominal sensors. Am J Obstet Ginecol 2011; 47:1-5.

[61]. A. Mahmoud, X. Zeng. A Novel Technique for Extraction Foetal Electrocardiogram using Adaptive Filtering and Simple Genetic Algorithm. Am J Biostat 2010; 2:75-81.

[62]. R. Sameni, C. Jutten, MB. Shamsollahi. What ICA Provides for ECG Processing: Application to Noninvasive Fetal ECG Extraction. IEEE ISSPIT 2006; 656-661.

[63]. R. Sameni, GD. Clifford, C. Jutten, MB. Shamsollahi. Multi-channel and noise modeling: application to maternal and fetal ECG signals. EURASIP J Adv Sig Pr 2007; 2007:1-14.

[64]. R. Vullings, C. Peters, M. Mischi, G. Oei, J. Bergmans. Maternal ECG removal from noninvasive fetal ECG recordings. IEEE EMBS 2006; 1394-1397.

[65]. S. Shaikh. Low Cost Multi-Lead ECG Signal Acquisition in Real Time with Telemetric Capability. UACEE IJAEEE 2012; 1:105-108.

[66]. G. Gargiulo, P. Bifulco, RA. Calvo, M. Cesarelli, C. Jin, A. McEwan, A. van Schaik. Noninvasive Electronic Biosensor Circuits and Systems. Intelligent and Biosensors 2010; 6:123-146.

[67]. SH. Fairclough, L. Venables, A. Tattersall. The influence of task demand and learning on the psychophysiological response. Int J Psychophysiol 2005; 56:171-184.

[68]. C. Marque, J. Duchˆene, S. Leclercq, G. Panczer, J. Chaumont. Uterine ehg processing for obstetrical monitoring," IEEE Trans Biomed Eng 1986; 33:1182-1187.

[69]. C. Rabotti, Characterization of uterine activity by electrohysterography. Phd thesis, Technische Universiteit Eindhoven, The Netherlands, 2010.

[70]. C. Rabotti, M. Mischi, JOEH. Van Laar, SG. Oei, JWM. Bergmans. Estimation of internal uterine pressure by joint amplitude and frequency analysis of electrohysterographic signals. Physiol Meas 2008; 29:829–841.

[71]. C. Buhimschi, MB. Boyle, RE. Garfield. Electrical activity of the human uterus during pregnancy as recorded from the abdominal surface. Obstet & Gynecol, 1997; 90:102–111.

[72]. SM. Martens, M. Mischi, SG. Oei, JWM. Bergmans. An improve adaptive powerline interference canceller for electrocardiography. IEEE Trans Biomed Eng 2006; 53:2220–2231.

[73]. TF. Oostendorp, A. van Oosterom, HW. Jongsma. The effect of change in the conductive medium on the fetal ECG throughout gestation. Clin Phys Physiol Meas 1989; 10:11–20.

[74]. TF. Oostendorp, A. van Oosterom. Electrical properties of tissues involved in the conduction of foetal ECG. Med Biol Eng Comput 1989; 27:322–324.

[75]. TF. Oostendorp, A. van Oosterom, HW. Jongsma. The fetal ECG throughout the second half of gestation. Clin Phys Physiol Meas 1989; 10:147–160.

[76]. J.G. Stinstra. Reliability of the fetal magnetocardiogram. Phd thesis, Universiteit Twente, The Netherlands, 2001.

[77]. JT. Oldenburg, M. Macklin. Changes in the conduction of the fetal electrocardiogram to the maternal abdominal surface during gestation. Am J Obstet Gynecol 1977; 129:425–433.

[78]. JA. Crowe, D. James, BR. Hayes-Gill, CW. Barratt, JF. Pieri. Fetal surveillance. International patent No: WO/2005/039410, 2004-10-13.

[79]. AR. Kahn. Transmission characteristics in fetal electrocardiography. Conf on Engineering, Medicine and Biology, USA, 1963; 134.

[80]. JB. Roche, EH. Hon. The fetal electrocardiogram v. comparison of lead systems. Am J Obstet Gynecol 1965; 92:1149–1159.

[81]. RA. Brace. Physiology of amniotic fluid regulation. Clin Obstet Gynecol 1997; 40:180–189.

[82]. M. Kotas, J. Jezewski, K. Horoba, T. Kupka. Detection of low amplitude fetal QRS complexes. IEEE EMBS 2008; 4764–4767.

[83]. F. Mochimaru, Y. Fujimoto, Y. Ishikawa. Detecting the fetal electrocardiogram by wavelet theory-based methods. Prog Biomed Res 2002; 7:185–193.

[84]. H. Hassanpour, A. Parsaei. Fetal ECG Extraction using Wavelet Transform. CIMCA 2006; 1–4.

[85]. PP. Kanjilal, S. Palit, G. Saha. Fetal ECG extraction from single-channel maternal ECG using singular value decomposition. IEEE Trans Biomed Eng 1997; 44:51–59.

[86]. B. Azzerboni, F. La Foresta, N. Mammone, FC. Morabito. A new approach based on wavelet-ICA algorithms for fetal electrocardiogram extraction. ESANN 2005:193–198.

[87]. P. Gao, Ee-C Chang, L. Wyse. Blind separation of fetal ECG from single mixture using SVD and ICA. ICICS PMC 2003; 3:1418–1422.

[88]. T. Schreiber, DT. Kaplan. Signal separation by nonlinear projections: The fetal electrocardiogram. APS 1996; 53:4326–4329.

[89]. M. Richter, T. Schreiber, DT. Kaplan. Fetal ECG extraction with nonlinear state-space projections. IEEE Trans Biomed Eng 1998; 45:133–137.

[90]. S. Muceli, D. Pani, L. Raffo. Non-Invasive Real-Time Fetal Ecg Extraction. A Block-on-Line DSP Implementation based on the JADE Algorithm. Biosignals 2008; 458-463.

[91]. J. Jezewski, A. Matonia, T. Kupka, D. Roj, R. Czabanski. Determination of fetal heart rate from abdominal signals: evaluation of beat-to-beat accuracy in relation to the direct fetal electrocardiogram. Biomed Tech 2012; 57:383–394.

[92]. R. Sameni, MB. Shamsollahi, C. Jutten. Filtering electrocardiogram signals using the extended kalman filter. IEEE EMBS 2005; 5639–5642.

[93]. MA. Hasan, MI. Ibrahimy, MBI. Reaz. Fetal ECG extraction from maternal abdominal ECG using neural network. J Softw Eng Appl 2009; 2:330–334.

[94]. J. Pan, WJ. Tompkins. A real-time QRS detection algorithm. IEEE Trans Bio-Med Eng 1985; 32:230–236.

[95]. M. Ungureanu, JWM Bergmans, SG. Oei, R. Strungaru. Fetal ECG extraction during labor using an adaptive maternal beat subtraction technique. Biomed Tech 2007; 52:56–60.

[96]. G. Welch, G. Bishop. An introduction to the Kalman filter. Siggraph 2001; 1–48.

[97]. GD. Clifford, L. Tarassenko. Quantifying errors in spectral estimates of HRV due to beat replacement and resampling. IEEE Trans Biomed Eng 2005; 52:630–638.

[98]. C. Peters, R. Vullings, J. Bergmans, G. Oei, P.Wijn. The effect of artifact correction on spectral estimates of heart rate variability. IEEE EMBC 2008; 2669–2672.

[99]. CM Bishop. Pattern recognition and machine learning, Springer Science Business, New York, USA, 2006.

[100]. DG. Clifford, I. Silva, J. Behar, GB. Moody. Non-invasive fetal ECG analysis. Physiol Meas 2014; 35:1521–1536.

[101]. M. Malik, K. Hnatkova, M. Sisakova, G. Schmidt. Subject specific heart rate dependency of electrocardiographic QT, PQ, and QRS intervals. J Electrocardiol 2008; 41:491-497.

[102]. HH. Abbas. Removing 0.5 Hz baseline wander from ECG signal using multistage adaptive filter. Eng Tech J 2011; 29:2312–28.

[103]. G. Umamaheswara Reddy, M. Muralidhar. Removal of electrode motion artifact in ecg signals using wavelet based threshold methods with grey incidence degree. Int J Electr Electron Eng 2012; 1:1–8.

[104]. S. Abbaspour, H. Gholamhosseini, M. Linden. Evaluation of wavelet based methods in removing motion artifact from ECG signal. Int Fed Med Biol Eng Proc 2015; 48:1–4

[105]. M. Sucheta, N. Kumaravel. Empirical mode decomposition based filtering techniques for powerline interference reduction in electrocardiogram using various adaptive structures and subtraction methods. Biomed Sig Process Control 2013; 8:575-85.

[106]. M. Blanco-Velasco, B. Weng, KE. Barner. ECG signal denoising and baseline wander correction based on the empirical mode decomposition. Comput Biol Med 2008; 38:1-13.

[107]. M. Ungureanu, W. Wolf. Basic aspects concerning the event-synchronous interference canceller. IEEE Trans Biomed Eng 2006; 53:2240–7.

[108]. AL. Goldberger, LAN. Amaral, L. Glass, JM. Hausdorff , PC Ivanov, RG. Mark, JE. Mietus, GB. Moody, CK. Peng, HE. Stanley. PhysioBank, physiotoolkit, and physionet: components of a new research resource for complex physiologic signals. Circulation 2000; 101:215–20.

[109]. M. Sarfraz, F. Li. Independent component analysis for motion artifacts removal from electrocardiogram. GPAI 2013; 1:49–55.

[110]. GB. Moody, W. Muldrow, RG. Mark. A noise stress test for arrhythmia detectors. Comput Cardiol 1984; 11:381–4 .

[111]. A. Agostinelli, A. Sbrollini, L. Burattini, S. Fioretti, F. Di Nardo, L. Burattini. Noninvasive Fetal Electrocardiography Part II: Segmented-Beat Modulation Method for Signal Denoising. TOBEJ (Submitted)

[112]. RG. Gallager. Principles of Digital Communication. MIT OpenCourseWare 2006; I:119-248.

[113]. R. Vullings, C. Peters, M. Mischi, R. Sluijter, G. Oei, J. Bergmans. Artifact reduction in maternal abdominal ECG recordings for fetal ECG estimation. IEEE EMBS 2007; 43-46.

[114]. IE. Sigurdardottir. R-wave detection algorithms using adult and fetal ECG signals. M. Thesis, Chalmers University of Technology, Gothenburg, Sweden 2013.

[115]. P. Rajput, B. Singh, P. Karan. Fetal heart monitor. Int J Sci Eng Res 2012; 3:1358-1364.

[116]. A. Agostinelli, I. Marcantoni, E. Moretti, A. Sbrollini, S. Fioretti, F. Di Nardo, L. Burattini. Noninvasive Fetal Electrocardiography Part I: Pan-Tompkins' Algorithm Adaptation to Fetal R-peak Identification. TOBEJ (Submitted)